AD-A210 262

Computing Induced Velocity Perturbations Due to a Helicopter Fuselage in a Free Stream

John D. Berry and Susan L. Althoff
Aerostructures Directorate
USAARTA-AVSCOM
Langley Research Center
Hampton, Virginia

Contents

Introduction

To understand and predict the complex flow associated with rotorcraft, particularly in forward flight, the elements contributing to the flow must be identified and properly modeled. The rotor and its wake are the major contributors to the flow field, and significant work has been performed to identify the effect of the lifting rotary wing on the flow field. A historical perspective of this work is presented in reference 1.

Rotor inflow has a significant effect on the performance of the rotor. Inflow is the effective flow seen at the rotor disk and is affected by several factors: the free-stream velocity, the rotor/wake induced velocities, and fuselage induced velocities. Rotor performance codes use inflow models that range from the assumption of uniform inflow to complex, time-varying, vortex filament, "free-wake" models and, generally, ignore the effects of the fuselage on the velocities seen by elements of the lifting rotor.

The fuselage affects the rotor inflow in two ways: the velocity perturbation due to the presence of the fuselage, and the velocity perturbations due to changes in the rotor wake. The effect of the velocity perturbation due to the fuselage can be modeled using potential-flow theory, whereas the effect of the fuselage on the rotor wake is a highly complex problem from which no simple models have been developed. To date, the effect of the fuselage on the flow field has been studied with a relatively limited effort. Several researchers have considered the effects of the fuselage both experimentally (refs. 2-9) and with analysis (refs. 10-17).

The effects of the fuselage have been modeled by previous researchers in various ways. The work of Crimi and Trenka (ref. 10) modeled both the rotor wake and the fuselage in predicting the downwash field of the helicopter. The source-panel method is used by Keys (ref. 5) for the fuselage effect on angle of attack at the rotor. An assessment of the fuselage effects on rotor performance and loads using a simple axisymmetric fuselage was made by Johnson and Yamauchi (ref. 15). The work of Ryan et al. (ref. 17) demonstrates the effect of modeling a region of separated flow from the fuselage on velocities at the rotor plane. The effect of the fidelity of fuselage modeling on the rotor-inflow velocities has not been demonstrated by any of the researchers.

An experimental rotorcraft program has been undertaken to provide detailed measurements of rotor inflow (refs. 18-25). These data have been used to evaluate the rotor-inflow models used by rotor performance codes (refs. 18 and 24). These flow field measurements were made with a two-component laser Doppler velocimeter over a helicopter model with a realistic, although simplified, fuselage. Data were also collected over the fuselage without a lifting rotor to assess the magnitude of the isolated fuselage perturbations.

The purpose of this study is to assess the effect of the fuselage used in the experimental rotorcraft program on the inflow velocity field. A potential-flow, source-panel method is used to predict the inflow velocity perturbations due to the fuselage for a fuselage with three levels of complexity, and these perturbations are compared with the experimental flow field measurements. Predictions of the velocity perturbations for the rotor conditions investigated in the experimental rotorcraft program are presented. The data and analyses presented in this report show the velocity perturbation due only to the presence of the fuselage since the data were collected and computed in the absence of the rotor. The use of these data presumes that superposition of fuselage and rotor/wake effects can be used to model the combined flow field.

Symbols

The symbols used in the basic report are given as follows:

A	influence coefficient matrix
a	aerodynamic influence coefficient (see eq. (2))
B	scalar array of boundary condition
$\vec{n}$	surface normal vector
O	occurrences
O_u, O_w	occurrences in u and w velocities, respectively (see table 1)
p	point on body of potential evaluation
q	source location on body
R	reference radius, Fuselage length/2, 3.33 ft
r	radial distance from hub center
r_m	rotor radius of specific rotor blade set
S	scalar array of source strength
U, W	velocity components (laser velocimeter), fps
u	tangential velocity perturbation (downstream tangent to rotor plane), fps
V_∞	free-stream speed, fps
$\vec{V}_\infty$	free-stream velocity vector, fps

v	lateral velocity perturbation (lateral tangent to rotor plane), fps
w	normal velocity perturbation (normal to rotor plane), fps
x, y, z	Cartesian coordinates
α	rotor-disk angle of attack, deg
σ	source strength; also standard deviation where indicated
ψ	rotor azimuth angle (counterclockwise from downstream), deg

Mathematical Formulation

The mathematical basis for the analysis code is classical potential flow. Green's theorem is used to describe the potential field as integrals of singularity functions over the boundaries of the flow. A source-panel method, based on the work of Hess and Smith (refs. 26 and 27), has been implemented for body configurations that can be modeled with quadrilateral panels. Appendix A contains the basic formulation of the relations between the strength of a distributed source over a quadrilateral panel and the velocity produced at any point in space. The relations shown in appendix A are implemented as a subroutine that computes a velocity vector for a panel geometry, strength, and field point.

The source-panel method has been in use for over 20 years and has an established record for analysis of incompressible potential flow. The implementation here uses existing mathematical relations with current computer-solution techniques not possible when the original formulation was implemented.

A computer program was developed to solve for the source strengths over arbitrary paneled shapes in the presence of uniform flow. The solution was developed by satisfying the no-penetration condition at each panel centroid. The form of this equation is

$$\sum_q d\vec{V}_q \cdot \vec{n}_p = -\vec{V}_\infty \cdot \vec{n}_p \qquad (1)$$

where $d\vec{V}_q$ is the portion of the velocity vector at p due to the source panel at q.

A system of linear equations can be formed for the unknown source strengths:

$$\begin{bmatrix} a_{11} & a_{12} & \cdots & a_{1N} \\ a_{21} & a_{22} & \cdot & a_{2N} \\ \vdots & \vdots & \ddots & \vdots \\ a_{N1} & a_{N2} & \cdots & a_{NN} \end{bmatrix} \begin{Bmatrix} \sigma_1 \\ \sigma_2 \\ \vdots \\ \sigma_N \end{Bmatrix} = \begin{Bmatrix} -\vec{V}_\infty \cdot \vec{n}_1 \\ -\vec{V}_\infty \cdot \vec{n}_2 \\ \vdots \\ -\vec{V}_\infty \cdot \vec{n}_N \end{Bmatrix}$$

$$(2)$$

In matrix notation, this system can be written as a coefficient matrix **A** that is multiplied by the unknown scalar array of the source strength **S** and set equal to the scalar array of the boundary condition **B**.

The elements of the coefficient matrix **A** are computed using the velocity-computing subroutine described above and detailed in appendix A, but substituting the value of unity for the source strength of the panel. The unknown scalar array of source strength **S** can be solved by the normal methods for linear systems.

In the specific program used for the analysis presented, the linear system is solved by lower-upper decomposition by Crout's algorithm with implicit partial pivoting and back substitution using the implementation of reference 28. Once the source strengths are known, the field point velocities are computed by the same subroutine used to compute the coefficient matrix elements. The program saves the decomposed coefficient matrix so that new strengths can be computed by changing the right-hand-side vector and returning to the back-substitution step for the unknown source strengths.

Experiment

Experimental measurements of the perturbation velocity due to a representative helicopter fuselage were made during a helicopter inflow-measurement program. The rotor-inflow data are reported in references 19–23. The isolated fuselage velocities are reported here. The experiment was conducted in the Langley 14- by 22-Foot Subsonic Tunnel. This facility is an atmospheric, closed-circuit tunnel designed specifically for high-lift and powered-model testing at low to moderate speeds. The facility is described in detail in references 29 and 30. The perturbation velocity measurements were made using a two-component laser velocimeter (refs. 31 and 32).

The fuselage shape used in this study is an analytic shape that can be parameterized using easily defined coordinates. The specific geometry is described in references 4 and 33, and the equations, their coefficients, and tabulated coordinates are given in appendix B. This geometry consists of a slender main body with a slender nacelle portion about the rotor shaft. The model is shown mounted for testing in figure 1; however, the measurements presented here were taken without the rotor blades.

The velocity measurements were made along the fuselage centerline 3 in. above the plane that would have been the rotor tip path plane if a rotor had been operating on the model. This includes an assumption of no oscillatory flapping about the rotor shaft axis, a steady coning of the rotor blades of 1.5°, and a

shaft angle tilt of 3° nose down. Figure 2 shows the locations used in the inflow investigation relative to the fuselage. The free-stream velocity was held at approximately 94 fps to simulate an advance ratio of 0.15 with an assumed tip speed of 624 fps. The fuselage attitude with respect to the rotor shaft was 2.5° nose up, giving the fuselage an effective angle of attack with respect to the free-stream velocity of 0.5° nose down. The assumed radius of the rotor blades r_m was 33.88 in.

The measured velocities are presented in table 1 as perturbation velocities normalized by the tunnel free-stream velocity and in the tip-path-plane reference system. The normal (u) and tangential (w) components of perturbation velocity are computed from the laser velocimeter components, U and W, by

$$u = (U - V_\infty)\cos\alpha + W\sin\alpha \qquad (3)$$

and

$$w = W\cos\alpha - (U - V_\infty)\sin\alpha \qquad (4)$$

The nondimensional mean velocities for the u- and w-components are listed, as well as the standard deviation σ and the number of samples or occurrences O that determine each average. The average tunnel free-stream velocity V_∞ for each data point is also listed.

It should be noted that the tunnel free-stream velocity was not determined using the laser velocimeter, but it was measured using wind-tunnel instrumentation. An error analysis of both laser velocimeter and tunnel velocity systems has been conducted, and the results are detailed in appendix C. The laser velocimeter measurements had a velocity accuracy from 1.19 to 1.80 percent for the test conditions of this experiment. The accuracy of the tunnel velocity measurements was approximately 8 percent of the free-stream velocity in this experiment. The tunnel-indicated free-stream velocity has been corrected based on the laser velocimeter measurement farthest from the body disturbance. This correction, detailed in appendix C, amounts to approximately 4 percent of the experimental free stream. The correction reduces the error associated with the free-stream velocities reported here to that of the laser velocimetry system. The large inaccuracy of the indicated tunnel velocity was found to be due to operator oversight and is applicable only for these reported data.

Results and Discussion

Three panel models of the experimental fuselage were constructed to predict the flow perturbations.

These predictions were made to compare with experimental results. The first model represents only the smooth portions of the experimental model, that is, the main fuselage shape and the faired nacelle shape. The resulting panel configuration for the first model is shown in figure 3 and is referred to as the ROBIN fuselage, which was derived from the rotor body interaction studies conducted at the Langley Research Center. (See refs. 2 and 4 for examples.) The code used to generate this basic fuselage shape is given in appendix B. The second and third models were constructed to assess the effect of more or less detail in the modeling of the fuselage and, in particular, the shaft and hub. The second model includes a simplified panel representation of the rotor shaft and hub. Because of the relative complexity of the hub and pitch change links, a radius was chosen for the shaft and hub body to represent the frontal area relative to the oncoming flow. The resulting panel configuration for the second model is shown in figure 4. The third model is a representation of the fuselage as an ellipsoid of equivalent fineness ratio relative to the fuselage width, in this case 1:8. The resulting panel configuration for the third model is shown in figure 5.

A comparison of the measured and computed velocity perturbations due to the fuselage along the measurement plane centerline is shown in figure 6. The figure also compares the predicted perturbation due to the three models for the fuselage. Two components of perturbation velocity will be presented, the normal component (relative to the plane of the rotor disk) and the tangential component (tangent to the rotor disk and directed downstream). The velocity ratios shown in this figure have the free-stream velocity removed from the local velocity and the result divided by the free-stream velocity. In figure 6(a) the normal component of the velocity perturbation is shown. In figure 6(b) the tangential component of the velocity perturbation is shown. The figures show a velocity ratio derived from the free-stream velocity and corrected as described in appendix C.

The velocity perturbation ahead of the hub shows good agreement with the measured experimental values, although all three fuselage models underestimate the normal component. The ellipsoid model underpredicts the flow by a wide margin, whereas the two ROBIN models have similar predictions at the most forward locations. As the hub is approached, the ROBIN fuselage and nacelle model does not predict the measured velocities as well as the model with the crude hub representation. However, close to the hub region, the crude model apparently overestimates the magnitude of the perturbations. Behind the hub the

models predict the normal component well, but they do not agree as well with the downstream component.

The disagreement between measured velocity perturbations and the predictions based on source-panel models behind the hub may be attributed to the large amount of unmodeled separated flow in this region of the flow. The existence of this separated region has been confirmed and is routinely accounted for in rotorcraft drag-estimation techniques such as that described by Keys (ref. 5). The flow over the aft portion of the fuselage is likely to be affected by both hub separation and perhaps some amount of fuselage separation. It is interesting to note that the simple ellipsoid fuselage shape comes closest to adequately predicting the downstream component of perturbation behind the hub. It is likely that the larger cross section of the ellipsoid in this region models the existence of separated flow in the aft section of the fuselage. With the exception of the two measurement locations closest to the hub, the ROBIN fuselage models, both without and with hub, predict the correct perturbation trend in the normal component. At the measurement location just ahead of the hub, the use of a hub model predicts the downstream component of perturbation well and shows the correct trend for the normal component prediction, although it overestimates the magnitude.

It is necessary to comment on the applicability of these computations. The computation and experiment are made in the absence of the rotor and its wake. The use of an isolated rotor/wake model with linear (i.e., superposition) inclusion of these fuselage effects ignores the possibility of wake deformation due to the fuselage and the effect of the rotor and wake on the source strength distribution on the fuselage surface. These nonlinear effects will be expected to change the magnitude and perhaps the local sign of the isolated fuselage interactions. This nonlinear effect must be properly modeled for complete rotor-fuselage interaction studies.

In a first-order sense, however, the assumption of linear superposition between the rotor wake and the fuselage may be a reasonable hypothesis. The reasoning for this assumption lies in the fact that the fuselage presents two disturbance types to the flow. The first disturbance is a volume disturbance that is modeled here as a source distribution on the surface. The second is a rotational disturbance that is formed by viscous action at the fuselage surface and is not modeled in this study. The volume disturbance of the fuselage has a direct effect on the wake trajectory but cannot change the strength of the wake elements. The rotational disturbance, however, has only a minor effect on the wake trajectory, but in close proximity, it can merge with the wake and thus

change its strength. If the rotational disturbance is weak, as is assumed here in the nonlifting fuselage assumption, the only effect on the wake is due to the trajectory perturbation. If the overall trajectory perturbations are small, the additional nonlinear effect of the fuselage on the rotor inflow is small. The actual magnitudes of these interacting disturbances must be assessed by either analysis or experiment to confirm this hypothesis.

For each of the experimental test conditions from references 19-23, which are summarized in table 2, the velocity perturbations are predicted using the source-panel method and the basic fuselage-panel configuration. The perturbations are predicted where the inflow velocity measurements occurred. The reference coordinates for locating the center of the radius/azimuth measurement plane are given relative to the fuselage coordinates. The basic fuselage, shown in figure 2, is $2R$ long with the x-coordinate of the nose station reference equal to zero. The fuselage midsection, from $x = 0.40R$ to $x = 0.80R$, is constant with the x-coordinate and symmetrical in the y- and z-coordinates, thus giving the center of this uniform section to be the reference $y = 0$ and $z = 0$. In this coordinate system, the center of the inflow measurement plane is located at $x = 0.685R$, $y = 0.0R$, and $z = 0.4074R$. The inclination of the fuselage to the measurement plane is the experimental 2.5° from the reference fuselage waterline.

To help correlate the computed perturbations to the experimental rotor-inflow data found in references 19-23, the significant differences in rotor radius and angle of attack are summarized in table 2. The tests were conducted in these references at slight variations in angle of attack to account for the propulsive force required from the rotor to trim at each forward speed. The results of the calculation for velocity perturbation for these rotor conditions for the basic fuselage-nacelle model are given in table 3 which contains four subtables—two for each of the significant angles of attack and two for each of the rotor reference lengths. (The shorter rotor was not tested, however, at the higher angle of attack.) Results similar to those found in table 3(a) for the fuselage-nacelle-hub model are given in table 4. Results for the ellipsoid model are given in table 5.

To assess the effect of the minor differences in test condition, figure 7 presents maps of the w-component of velocity perturbation for three test conditions: (1) $r_m/R = 0.8470$ and $\alpha = -3.0°$ (referred to as the reference test condition); (2) $r_m/R = 0.8470$ and $\alpha = -4.0°$; and (3) $r_m/R = 0.8125$ and $\alpha = -3.0°$. The change in rotor radius is simply a scaling of the radial dimension of the figure, since the rotor is not present. The variation in w-distribution between

conditions (1) and (2) is small and diminishes away from the hub.

Maps of the distribution of predicted velocity perturbations in the u-, v-, and w-components for the reference condition are presented in figures 8, 9, and 10, respectively. In each of these figures, the predictions from the three modeling configurations are given in parts (a), (b), and (c). Part (a) is the map from a panel configuration for the fuselage-nacelle combination only, part (b) is a map from the fuselage-nacelle-hub panel configuration, and part (c) is a map from the ellipsoid fuselage configuration.

The effect of modeling the regions near the top of the fuselage on the tangential flow can be seen in figure 8. For a reasonable model of the fuselage and nacelle, the accelerated region is centered over the rotor shaft, thus coinciding with the closest region of the fuselage and amounting to 3 percent of free-stream velocity. For the rough approximation to the rotor hub and fuselage, perturbation velocities approaching 10 percent of free stream are predicted at the sides of the hub model, but they reduce quickly away from the hub to levels comparable with the fuselage-nacelle model. For the ellipsoid, only a moderate (1 percent of free stream) velocity increase is predicted over the thickest portion of the fuselage. The ellipsoid model, however, showed better correlation with the measured velocities aft of the hub (fig. 6).

The effect of fuselage modeling on the lateral flow can be seen in figure 9. For the fuselage-nacelle model, the regions of maximum perturbation velocity are antisymmetrically distributed about the rotor shaft and amount to less than 2 percent of free-stream velocity. The regions of largest perturbation are found at approximately 1/4 radius on either side of the fuselage centerline at approximately 1/4 radius ahead of the hub. For the approximation to the rotor hub and fuselage, velocities approaching 5 percent of free stream are predicted at the diagonal quadrants of the hub model, but they reduce quickly away from the hub to levels comparable with the fuselage-nacelle model. The computed values of the magnitudes of lateral velocity perturbation are less than the predicted values for either the normal component or tangential component. For the ellipsoid, only a small (half of a percent of free stream) velocity perturbation is predicted over either side of the front portion of the fuselage.

The effect of modeling the fuselage on the normal velocity perturbations can be seen in figure 10. For the fuselage and nacelle model, upflow occurs over the forward half of the measurement disk with the highest perturbation, about 4 percent of free stream, along the centerline about 1/3 radius ahead of the

hub. With the same model, a 3-percent downflow is found about 1/3 radius behind the hub. For the approximation to the rotor hub and fuselage, upflow perturbations approaching 15 percent of free stream are predicted ahead of the hub model and downflow of 13 percent behind the hub, but they reduce quickly away from the hub to levels comparable with the fuselage-nacelle model. For the ellipsoid, only a moderate (2 percent of free stream) perturbation is predicted over the fuselage nose, with the zero normal component line behind the hub at the location of maximum fuselage thickness.

The high normal velocity perturbation predicted close to the hub can be attributed to the panels placed vertically around the hub. There are no vertical faces on the experimental hub. In figure 6(a), the difference between the hub and fuselage prediction and the experimental value at $\psi = 180°$ and $r/r_m = 0.20$ verifies that the hub model produces too much normal component in the close proximity of the hub. The normal-component prediction shows agreement at the next experimental station, $r/r_m = 0.50$. The model without the hub and with the model with the hub, respectively, predict approximately 3 percent and 15 percent of free-stream normal perturbation. The experimental value of normal perturbation at $r/r_m = 0.20$ is approximately 8 percent of the free stream, thus indicating that the model used for the hub induces twice the appropriate perturbation in its local vicinity.

Concluding Remarks

The velocity field of a representative helicopter fuselage in a free stream is computed. Perturbation velocities due to the fuselage are computed in a plane above the location of the helicopter rotor (rotor removed) corresponding to experimental rotor-inflow velocities measured. Velocity measurements made with a laser velocimeter over an isolated helicopter fuselage with hub are presented and compared with the velocities computed using three fuselage panel models. The models used in this study were a representative helicopter fuselage both with and without a hub model and a body-of-revolution fuselage.

The velocity perturbations computed using the source-panel method on the two helicopter fuselage shapes agree well with the measured velocity field except in the close vicinity of the rotor hub. In the hub region, modeling of the effective fuselage is difficult without knowing the extent of separation and the effective source shape of the rotating hub. The effects of the fuselage perturbations are not well-predicted with a body-of-revolution fuselage.

The effects of slight changes in fuselage attitude (needed for rotor trim) are shown to be insignificant in the fuselage induced velocity perturbations.

The normal velocity perturbations due to the fuselage at the plane of the inflow measurements have magnitudes of less than 8 percent of free-stream velocity. The tangential velocity perturbations due to the fuselage in the same plane have magnitudes of less than 6 percent of free-stream velocity. The lateral velocity perturbations due to the fuselage in the same plane have an antisymmetric pattern with magnitudes less than either the normal or tangential components of velocity perturbation. Computed data are tabulated for conditions corresponding to reported experimental inflow data.

Appendix A

Source-Panel Formulation

Symbols

The symbols used in this appendix are given as follows:

A area of a panel

d length of panel edge

$e, h, \mathcal{P}, \mathcal{Q}$ simplifying expressions (see subsequent text)

I panel inertia (see subsequent text)

k subscript used as panel corner identifier

M panel moment (see subsequent text)

m panel edge slope

$\vec{n}$ surface normal vector

P point in space of potential evaluation

p point on body of potential evaluation

q source location on body

r distance from source to evaluation point

S surface of body

$\vec{V}$ velocity with components V_x, V_y, and V_z

$\vec{V}_\infty$ free-stream velocity vector

w simplifying expression in mid-field calculations (see eq. (A13)), $1/r$

x, y, z Cartesian coordinates

ξ, η coordinates in plane of panel

σ source strength

φ velocity potential

Potential Formulation

This appendix describes the background and specific relations between distributed source panels and their velocity field. The basis for the source-panel method is the solution for the potential field by the method of Green's theorem. The specific solution for Laplace's equation is that of a potential source.

For irrotational incompressible flow, the governing equation, expressed in terms of velocity potential φ, is:

$$\nabla^2 \varphi = 0 \qquad (A1)$$

where ∇ denotes the common del operator and the velocity potential φ is related to the velocity by

$$\vec{V} = -\vec{\nabla}\varphi \qquad (A2)$$

The potential at any point P in space due to a closed surface S of potential source $\sigma(q)$, where q is a location on S, can be written as

$$\varphi(x, y, z) = \iint\limits_S \frac{\sigma(q)}{r(P, q)} dS \qquad (A3)$$

as shown in reference 26. As the point of integration approaches the surface, the integrand becomes singular. At the surface point p, the singular value is determined to be

$$\frac{\partial \varphi}{\partial n} = -2\pi\, \sigma(p) + \iint\limits_S \frac{\partial}{\partial n}\left[\frac{1}{r(p, q)}\right] \sigma(q)\, dS \quad (A4)$$

where $\partial/\partial n$ is the partial derivative normal to the surface. The resulting integral equation for the source values is

$$2\pi\, \sigma(p) - \iint\limits_S \frac{\partial}{\partial n}\left[\frac{1}{r(p, q)}\right] \sigma(q)\, dS = -\vec{n}(p) \cdot \vec{V}_\infty$$

$$(A5)$$

The panel method of discretizing the surface reduces the surface integration to a small panel region that can be assumed to be planar, thus making direct integration possible. The method used here is that developed by Hess and Smith (refs. 26 and 27). A planar panel is projected from the four corners of the panel quadrilateral.

The panel geometry is defined by its four corner points, numbered clockwise as 1, 2, 3, 4. The coordinate system ξ, η will be used for locations on the panel and is mapped from the x, y space. The point at which the induced velocity is to be found is given by its coordinates in panel local notation x, y, z.

The potential at x, y, z is given by

$$\varphi = \iint\limits_A \frac{1}{r} dA$$

$$= \iint\limits_A \frac{d\xi\, d\eta}{\sqrt{(x - \xi)^2 + (y - \eta)^2 + z^2}} \qquad (A6)$$

Here, the value of r is the distance from P to the point on the panel with coordinates $(\xi, \eta, 0)$. The area of integration A is the surface of the panel. The components of induced velocity can now be computed:

$$V_x = -\frac{\partial \varphi}{\partial x}$$
$$= \iint_A \frac{x - \xi}{r^3} d\xi \, d\eta \tag{A7}$$

$$V_y = -\frac{\partial \varphi}{\partial y}$$
$$= \iint_A \frac{y - \eta}{r^3} d\xi \, d\eta \tag{A8}$$

$$V_z = -\frac{\partial \varphi}{\partial z}$$
$$= \iint_A \frac{z}{r^3} d\xi \, d\eta \tag{A9}$$

The relationship between induced velocity and panel geometry is given by Hess and Smith and is in three forms which reduce the amount of computation needed based on the distance from the panel. In the "near-field," the form takes an exact representation of the velocity induced by a planar-distributed source panel. The near-field is defined as the region where the square of the distance from the panel centroid is less than six times the square of the larger panel diagonal. In the "mid-field," the form taken consists of the lower-order terms of an expansion of the exact solution about the panel centroid. The mid-field is defined as the region where the square of the distance from the panel centroid is between 6 and 16 times the square of the larger panel diagonal. In the "far-field," the form used is the velocity due to a point source at the panel centroid. The far-field is defined as the region where the square of the distance from the panel centroid exceeds 16 times the square of the larger panel diagonal.

Near-Field

The quadrilateral source panel is divided into two triangular regions of integration. After considerable manipulation, the resulting formulas for the three induced components of velocity at x, y, z are written as

$$V_x = \frac{\eta_2 - \eta_1}{d_{12}} \log \left(\frac{r_1 + r_2 - d_{12}}{r_1 + r_2 + d_{12}} \right)$$
$$+ \frac{\eta_3 - \eta_2}{d_{23}} \log \left(\frac{r_2 + r_3 - d_{23}}{r_2 + r_3 + d_{23}} \right)$$
$$+ \frac{\eta_4 - \eta_3}{d_{34}} \log \left(\frac{r_3 + r_4 - d_{34}}{r_3 + r_4 + d_{34}} \right)$$
$$+ \frac{\eta_1 - \eta_4}{d_{41}} \log \left(\frac{r_4 + r_1 - d_{41}}{r_4 + r_1 + d_{41}} \right) \tag{A10}$$

$$V_y = \frac{\xi_i - \xi_2}{d_{12}} \log \left(\frac{r_1 + r_2 - d_{12}}{r_1 + r_2 + d_{12}} \right)$$
$$+ \frac{\xi_2 - \xi_3}{d_{23}} \log \left(\frac{r_2 + r_3 - d_{23}}{r_2 + r_3 + d_{23}} \right)$$
$$+ \frac{\xi_3 - \xi_4}{d_{34}} \log \left(\frac{r_3 + r_4 - d_{34}}{r_3 + r_4 + d_{34}} \right)$$
$$+ \frac{\xi_4 - \xi_1}{d_{41}} \log \left(\frac{r_4 + r_1 - d_{41}}{r_4 + r_1 + d_{41}} \right) \tag{A11}$$

$$V_z = \tan^{-1} \left(\frac{m_{12} e_1 - h_1}{z r_1} \right) - \tan^{-1} \left(\frac{m_{12} e_2 - h_2}{z r_2} \right)$$
$$+ \tan^{-1} \left(\frac{m_{23} e_2 - h_2}{z r_2} \right) - \tan^{-1} \left(\frac{m_{23} e_3 - h_3}{z r_3} \right)$$
$$+ \tan^{-1} \left(\frac{m_{34} e_3 - h_3}{z r_3} \right) - \tan^{-1} \left(\frac{m_{34} e_4 - h_4}{z r_4} \right)$$
$$+ \tan^{-1} \left(\frac{m_{41} e_4 - h_4}{z r_4} \right) - \tan^{-1} \left(\frac{m_{41} e_1 - h_1}{z r_1} \right) \tag{A12}$$

where the panel edge lengths are given by

$$d_{12} = \sqrt{(\xi_2 - \xi_1)^2 + (\eta_2 - \eta_1)^2}$$

$$d_{23} = \sqrt{(\xi_3 - \xi_2)^2 + (\eta_3 - \eta_2)^2}$$

$$d_{34} = \sqrt{(\xi_4 - \xi_3)^2 + (\eta_4 - \eta_3)^2}$$

$$d_{41} = \sqrt{(\xi_1 - \xi_4)^2 + (\eta_1 - \eta_4)^2}$$

the edge slopes are given by

$$m_{12} = \frac{\eta_2 - \eta_1}{\xi_2 - \xi_1} \qquad m_{23} = \frac{\eta_3 - \eta_2}{\xi_3 - \xi_2}$$

$$m_{34} = \frac{\eta_4 - \eta_3}{\xi_4 - \xi_3} \qquad m_{41} = \frac{\eta_1 - \eta_4}{\xi_1 - \xi_4}$$

and the simplifying terms relative to the four corners (with $k = 1, 2, 3, 4$) are given as

$$r_k = \sqrt{(x - \xi_k)^2 + (y - \eta_k)^2 + z^2}$$

$$e_k = z^2 + (x - \xi_k)^2$$

$$h_k = (y - \eta_k)(x - \xi_k)$$

Mid-Field

The cost of computing the exact contribution of the distributed source can be reduced by simplifying the equation outside the field where exact solution is important. The near-field solution can be simplified by using a multipole expansion for the integrand of equation (A6). By expanding at the panel centroid, i.e., $\xi = \eta = 0$, the geometry of the panel is eliminated from the calculation. The integrand being expanded is

$$w = \frac{1}{r} = \frac{1}{\sqrt{x^2 + y^2 + z^2}} \qquad \text{(A13)}$$

This expansion, to terms of second order, is given as

$$\varphi = Aw - (M_x w_x + M_y w_y)$$
$$+ \frac{1}{2}(I_{xx} w_{xx} + 2I_{xy} w_{xy} + I_{yy} w_{yy}) + \cdots \quad \text{(A14)}$$

where

$$A = \iint_A d\xi \, d\eta$$

$$M_x = \iint_A \xi \, d\xi \, d\eta \qquad M_y = \iint_A \eta \, d\xi \, d\eta$$

$$I_{xx} = \iint_A \xi^2 \, d\xi \, d\eta \qquad I_{xy} = \iint_A \xi\eta \, d\xi \, d\eta$$

$$I_{yy} = \iint_A \eta^2 \, d\xi \, d\eta$$

Using this expansion and forming the velocities from the directional derivatives of the potential, the velocities can be computed from

$$V_x = -\frac{\partial \varphi}{\partial x}$$

$$= -\left(Aw_x + \frac{1}{2}I_{xx} w_{xxx} + I_{xy} w_{xxy} + \frac{1}{2}I_{yy} w_{xyy} \right)$$
$$\text{(A15)}$$

$$V_y = -\frac{\partial \varphi}{\partial y}$$

$$= -\left(Aw_y + \frac{1}{2}I_{xx} w_{xxy} + I_{xy} w_{xyy} + \frac{1}{2}I_{yy} w_{yyy} \right)$$
$$\text{(A16)}$$

$$V_z = -\frac{\partial \varphi}{\partial z}$$

$$= -\left[Aw_z + \frac{1}{2}I_{xx} w_{xxz} + I_{xy} w_{xyz} + \frac{1}{2}I_{yy} w_{yyz} \right]$$
$$\text{(A17)}$$

where the quantities A, I_{xx}, I_{xy}, and I_{yy} are given by the geometry and defined above. The derivatives of w are found to be

$$w_x = -x/r^3$$

$$w_y = -y/r^3$$

$$w_z = -z/r^3$$

$$w_{xxx} = 3x(3\mathcal{P} + 10x^2)/r^7$$

$$w_{xxy} = 3y\mathcal{P}/r^7$$

$$w_{xyy} = 3x\mathcal{Q}/r^7$$

$$w_{yyy} = 3y(3\mathcal{Q} + 10y^2)/r^7$$

$$w_{xxz} = 3z\mathcal{P}/r^7$$

$$w_{xyz} = -15xyz/r^7$$

$$w_{yyz} = 3z\mathcal{Q}/r^7$$

where

$$\mathcal{P} = y^2 + z^2 - 4x^2$$

$$\mathcal{Q} = x^2 + z^2 - 4y^2$$

Far-Field

In the far-field, the distribution of the source is of no significance; only the lumped effect, i.e., point source, is necessary. The point-source model for the effect of panel with unit source strength in the far-field can be expressed as

$$V_x = A(x - x_0)/r^3 \qquad \text{(A18)}$$

$$V_y = A(y - y_0)/r^3 \qquad \text{(A19)}$$

$$V_z = A(z - z_0)/r^3 \qquad \text{(A20)}$$

Here, the subscript 0 indicates the panel centroid.

Appendix B

Fuselage Geometry Description

The fuselage described for the experimental program is referred to as the ROBIN fuselage, derived from an earlier rotor body interaction program. The purpose in creating this fuselage shape was to have an analytically derived shape that could be recreated mathematically with little effort.

Symbols

The symbols used in this appendix are given as follows:

A	scale factor in x
B	scale factor in y
C	dimensional constant
$C_1, \cdots, C_8$	equation coefficient array
H	fuselage height
m	power constant in y
N	cross-section (elliptic) power constant
n	power constant in x
R	reference radius
r	radius in yz-plane
W	fuselage width
x, y, z	Cartesian coordinates
x_0	initial offset in x
y_0	initial offset in y
Z_0	offset in z (camber line)
ϕ	angle in yz-plane

General Equation

The fuselage shape is derived from the superellipse equation of the form

$$\left(\frac{x + x_0}{A}\right)^n + \left(\frac{y + y_0}{B}\right)^m = C \quad (B1)$$

where n and m are not of necessity equal to 2, an integer, or to each other. Also, A, B, C, x_0, and y_0 are constants. The fuselage is parameterized by the longitudinal station coordinate x where the cross-section y- and z-coordinates are defined by functions of height H, width W, camber line Z_0, and elliptic power N. These defining values are found by solving the superellipse equation for y in terms of x:

$$y = F(x) = B\left[C - \left(\frac{x + x_0}{A}\right)^n\right]^{1/m} - y_0 \quad (B2)$$

To compute fuselage geometry, an array of geometry coefficients is used for each of the separate fuselage elements. This array, C_1 to C_8, is related to the defining equation parameters by

$$C_1 = C \quad C_2 = * \quad C_3 = x_0 \quad C_4 = A$$
$$C_5 = n \quad C_6 = -y_0 \quad C_7 = B \quad C_8 = m$$

Note that the constant C_2 is arbitrary (*).

The cross-section parameters H, W, Z_0, and N are all treated as functions $F(x)$ with an independent set of C_1 to C_8 coefficients. The actual cross-section coordinates (y, z) are defined in polar coordinates (r, ϕ) from the superellipse equation with

$$y + y_0 = r \cos \phi \quad (B3)$$

$$x + x_0 = r \sin \phi \quad (B4)$$

and with $C = 1$ and $n = m = N$. Solving for r, this relation becomes

$$r = \left[\frac{(AB)^N}{(A \sin \phi)^N + (B \cos \phi)^N}\right]^{1/N} \quad (B5)$$

The coordinates of the fuselage can now be derived in terms of longitudinal station x and cylindrical coordinate ϕ.

The ROBIN fuselage is made of four body and two nacelle elements with the coefficients given in table B1. A listing for a FORTRAN program that generates the ROBIN fuselage is also given in table B1. The output of this program must be edited to match the nacelle edge to the fuselage seam so that aligning control points will be coincident between the nacelle and fuselage. A table of the fuselage-nacelle control points used in this study is given in table B2.

For the portion of the study involving the effects of a hub model, a simplified hub geometry was patched into the paneled ROBIN geometry described above. The fuselage-nacelle-hub control points used are given in table B3.

Table B1. Coefficients for Fuselage Generation and Computer Listing

Function	x/R	C_1	C_2	C_3	C_4	C_5	C_6	C_7	C_8
Main fuselage parameters
H	$0 \rightarrow 0.4$	1.000	−1.000	−0.400	0.400	1.800	0	0.250	1.800
W		1.000	−1.000	−.400	.400	2.000	0	.250	2.000
Z_0		1.000	−1.000	−.400	.400	1.800	−.080	.080	1.800
N		2.000	3.000	0	.400	1.000	0	1.000	1.000
H	$0.4 \rightarrow 0.8$	0.250	0	0	0	0	0	0	0
W		.250	0	0	0	0	0	0	0
Z_0		0	0	0	0	0	0	0	0
N		5.000	0	0	0	0	0	0	0
H	$0.8 \rightarrow 1.9$	1.000	−1.000	−0.800	1.100	1.500	0.050	0.200	0.600
W		1.000	−1.000	−.800	1.100	1.500	.050	.200	.600
Z_0		1.000	−1.000	−.800	1.100	1.500	.040	−.040	.600
N		5.000	−3.000	−.800	1.100	1.000	0	0	0
H	$1.9 \rightarrow 2.0$	1.000	−1.000	−1.900	0.100	2.000	0	0.050	2.000
W		1.000	−1.000	−1.900	.100	2.000	0	.050	2.000
Z_0		.040	0	0	0	0	0	0	0
N		2.000	0	0	0	0	0	0	0
Pylon parameters
H	$0.4 \rightarrow 0.8$	1.000	−1.000	−0.800	0.400	3.000	0	0.200	3.000
W		1.000	−1.000	−.800	.400	3.000	0	.172	3.000
Z_0		.125	0	0	0	0	0	0	0
N		5.000	0	0	0	0	0	0	0
H	$0.8 \rightarrow 1.018$	1.000	−1.000	−0.800	0.218	2.000	0	0.200	2.000
W		1.000	−1.000	−.800	.218	2.000	0	.172	2.000
Z_0		1.000	−1.000	−.800	1.100	1.500	.065	.060	.600
N		5.000	0	0	0	0	0	0	0

```
      program ROBIN
c        correction from the coefficients in TM 80051   (JDB-88)
      real xor(50),ch(6,8),cw(6,8),cz0(6,8),cn(6,8)
      character*8 labxor(6)
      data labxor/'0.0->0.4','0.4->0.8','0.8->1.9',
     +           '1.9->2.0','0.4->0.8','~> 1.018'/
      data xor/0.00, 0.04, 0.08, 0.12, 0.16, 0.24, 0.28, 0.32,
     +          0.40, 0.45, 0.56, 0.80, 0.96,1.018, 1.28, 1.48,
     +          1.72, 1.90, 1.96, 2.00,30*0.0/
      data ch/ 1.0, .25, 1.0, 1.0, 1.0, 1.0,
     +         -1.0, 0.0,-1.0,-1.0,-1.0,-1.0,
     +         -0.4, 0.0,-0.8,-1.9,-0.8,-0.8,
     +          0.4, 0.0, 1.1, 0.1, 0.4,.218,
     +          1.8, 0.0, 1.5, 2.0, 3.0, 2.0,
     +          0.0, 0.0, .05, 0.0, 0.0, 0.0,
     +          0.25,0.0, 0.2, .05, 0.2, 0.2,
     +          1.8, 0.0, 0.6, 2.0, 3.0, 2.0/
      data cw/ 1.0, .25, 1.0, 1.0, 1.0, 1.0,
     +         -1.0, 0.0,-1.0,-1.0,-1.0,-1.0,
     +         -0.4, 0.0,-0.8,-1.9,-0.8,-0.8,
     +          0.4, 0.0, 1.1, 0.1, 0.4,.218,
     +          2.0, 0.0, 1.5, 2.0, 3.0, 2.0,
     +          0.0, 0.0,0.05, 0.0, 0.0, 0.0,
     +          .25, 0.0, 0.2, .05,.172,.172,
     +          2.0, 0.0, 0.6, 2.0, 3.0, 2.0/
      data cz0/1.0, 0.0, 1.0, .04,.125, 1.0,
     +         -1.0, 0.0,-1.0, 0.0, 0.0,-1.0,
     +         -0.4, 0.0,-0.8, 0.0, 0.0,-0.8,
     +          0.4, 0.0, 1.1, 0.0, 0.0, 1.1,
     +          1.8, 0.0, 1.5, 0.0, 0.0, 1.5,
     +         -.08, 0.0, .04, 0.0, 0.0,.065,
     +          .08, 0.0,-.04, 0.0, 0.0, .06,
     +          1.8, 0.0, 0.6, 0.0, 0.0, 0.6/
      data cn/ 2.0, 5.0, 5.0, 2.0, 5.0, 5.0,
     +         3.0, 0.0,-3.0, 0.0, 0.0, 0.0,
     +         0.0, 0.0,-0.8, 0.0, 0.0, 0.0,
     +         0.4, 0.0, 1.1, 0.0, 0.0, 0.0,
     +         1.0, 0.0, 1.0, 0.0, 0.0, 0.0,
     +         0.0, 0.0, 0.0, 0.0, 0.0, 0.0,
     +         1.0, 0.0, 0.0, 0.0, 0.0, 0.0,
     +         1.0, 0.0, 0.0, 0.0, 0.0, 0.0/
c
c -- print the coefficient table (per tm80051)
      open(100,file='robin.tab',status='unknown')
      write(100,'(/////,30x,''fuselage parameters''//)')
      write(100,1005)
      write(100,'(5x,
     +       ''function  x/r      c1     c2     c3     c4     c5'',
     +       ''   c6     c7     c8'')')
      write(100,1005)
      do j=1,4
        write(100,1001)labxor(j),(ch(j,i),i=1,8)
        write(100,1002)(cw(j,i),i=1,8)
```

```
        write(100,1003)(cz0(j,i),i=1,8)
        write(100,1004)(cn(j,i),i=1,8)
      end do
      write(100,'(/////,32x,''pylon parameters''//)')
      write(100,1005)
      do j=5,6                                                          60
        write(100,1001)labxor(j),(ch(j,i),i=1,8)
        write(100,1002)(cw(j,i),i=1,8)
        write(100,1003)(cz0(j,i),i=1,8)
        write(100,1004)(cn(j,i),i=1,8)
      end do
      close(100)
 1001 format(8x,'h',2x,a8,1x,8f7.3)
 1002 format(8x,'w',11x,8f7.3)
 1003 format(8x,'z0',10x,8f7.3)
 1004 format(8x,'n',11x,8f7.3/)                                         70
 1005 format(5x,71('-'))
c
      call interact(ch,cw,cz0,cn)
c      if (1.eq.1) stop 'temporary stop'
      twopi = 8*atan(1.0)
c           6.28318
      open(101,file='robin.tmp',status='unknown')
      do i=2,20
        if (xor(i) .lt. 0.4) ix = 1
        if (xor(i) .ge. 0.4 .and. xor(i) .lt. 0.8) ix = 2               80
        if (xor(i) .ge. 0.8 .and. xor(i) .lt. 1.9) ix = 3
        if (xor(i) .ge. 1.9) ix = 4
        xn=geom(cn,ix,xor(i))
        xz0=geom(cz0,ix,xor(i))
        xw=geom(cw,ix,xor(i))
        xh=geom(ch,ix,xor(i))
c
c  -- first strip of zeros
        if (i.eq.2) then
            do j=1,17                                                   90
                k = 0
                if (j .eq. 1) k = 2
                write(101,100)xor(1),0.,geom(cz0,1,xor(1)),k,0
            end do
        end if
        do j=1,17
            th = twopi*(j-1)/16.
            k = 0
            if (j .eq. 1) k = 1
            sth = sin(th)                                               100
            cth = cos(th)
c
            denom = (abs(xh*sth)**xn + abs(xw*cth)**xn)**(1./xn)
            rval = .5*xh*xw/denom
c
            xval = xor(i)
            yval = rval*sth
            zval = xz0 + rval*cth
```

13

```fortran
c
              write(101,100)xval,yval,zval,k,0
           end do
           if (i.eq.20) then
              do j=1,17
                 k = 0
                 if (j .eq. 1) k = 1
                 write(101,100)xor(20),0.,geom(cz0,4,xor(20)),k,0
              end do
           end if
        end do
c
c -- now for the 'dog-house'
        do i=1,6
           indx = i+8
           ix=5
           if (i.gt.4) ix=6
           xn=geom(cn,ix,xor(indx))
           xz0=geom(cz0,ix,xor(indx))
           xw=geom(cw,ix,xor(indx))
           xh=geom(ch,ix,xor(indx))
c
c -- first strip of zeros
           if (i.eq.1) then
              do j=1,9
                 k = 0
                 if (j .eq. 1) k = 2
                 write(101,100)xor(indx),0.,geom(cz0,ix,xor(indx)),k,0
              end do
           else if (i .eq. 6) then
              do j=1,9
                 k = 0
                 if (j .eq. 1) k = 1
                 write(101,100)xor(indx),0.,geom(cz0,ix,xor(indx)),k,0
              end do
           else
              do j=1,9
                 th = .5*twopi*(9-j)/8.
                 k = 0
                 if (j .eq. 1) k = 1
                 sth = sin(th)
                 cth = cos(th)
c
                 denom = (abs(xh*sth)**xn + abs(xw*cth)**xn)**(1./xn)
                 rval = .5*xh*xw/denom
c
                 xval = xor(indx)
                 yval = rval*cth
                 zval = xz0 + rval*sth
c
                 write(101,100)xval,yval,zval,k,0
              end do
           end if
        end do
```

110

120

130

140

150

160

```
c
      close(101)
      stop 'done'
100   format(3f10.3,2i1)
      end
c
      real function VALU(coef,ix,xval)                                    VALU
      real coef(6,8)                                                       170
      valu= coef(ix,6)
      if (coef(ix,8) .ne. 0.) then
          x1=(xval-coef(ix,3))/coef(ix,4)
          x2=coef(ix,1)-coef(ix,2)*x1**coef(ix,5)
          valu = valu + coef(ix,7)*x2**(1./coef(ix,8))
      end if
      return
      end
c
      real function GEOM(coef,ix.xval)                                    GEOM
      real coef(6,8)                                                       181
      if (coef(ix,4) .eq. 0.) then
          geom= coef(ix,1)
      else
          x1 = coef(ix,1)+coef(ix,2)*(abs((xval+coef(ix,3))
     +          /coef(ix,4)))**coef(ix,5)
          geom = x1
          if (coef(ix,8) .eq. 0. .or. coef(ix,8) .eq. 1.0) return
          geom = coef(ix,7)*(abs(x1))**(1.0/coef(ix,8))+coef(ix,6)
      end if                                                               190
      return
      end
c
      subroutine INTERACT(co1,co2,co3,co4)                            INTERACT
      real co1(6,8),co2(6,8),co3(6,8),co4(6,8)
c
      write(6,*) ' interactive mode: '
   10 write(6,*) ' enter segment (1-6) and x station:'
      read(5,*,end=99)iseg,x
c                                                                          200
      write(6,*) ' dimensions are:'
      write(6,*) '      height: ',geom(co1,iseg,x)
      write(6,*) '       width: ',geom(co2,iseg,x)
      write(6,*) '    z offset: ',geom(co3,iseg,x)
      write(6,*) '       power: ',geom(co4,iseg,x)
c
      go to 10
c
   99 continue
      return                                                              210
      end
```

Table B2. ROBIN Fuselage-Nacelle Geometry

(a) Element 1

Strip	x	y	z	Strip	x	y	z
0	0	0	−0.080	2	0.080	0	0.031
						−.027	.029
						−.054	.018
						−.071	−.007
						−.075	−.037
						−.071	−.066
						−.054	−.091
						−.027	−.102
						0	−.104
						.027	−.102
						.054	−.091
						.071	−.066
						.075	−.037
						.071	−.007
						.054	.018
						.027	.029
						0	.031
1	0.040	0	−0.003	3	0.120	0	0.055
		−.019	−.005			−.033	.054
		−.037	−.013			−.067	.040
		−.051	−.029			−.086	.009
		−.054	−.050			−.089	−.027
		−.051	−.071			−.086	−.063
		−.037	−.087			−.067	−.095
		−.019	−.095			−.033	−.108
		0	−.097			0	−.110
		.019	−.095			.033	−.108
		.037	−.087			.067	−.095
		.051	−.071			.086	−.063
		.054	−.050			.089	−.027
		.051	−.029			.086	.009
		.037	−.013			.067	.040
		.019	−.005			.033	.054
		0	−.003			0	.055

Strip	x	y	z	Strip	x	y	z
4	0.160	0	0.075	6	0.280	0	0.112
		−.038	.073			−.048	.111
		−.078	.058			−.100	.094
		−.098	.021			−.118	.044
		−.100	−.020			−.119	−.005
		−.098	−.060			−.118	−.054
		−.078	−.098			−.100	−.105
		−.038	−.113			−.048	−.121
		0	−.114			0	−.122
		.038	−.113			.048	−.121
		.078	−.098			.100	−.105
		.098	−.060			.118	−.054
		.100	−.020			.119	−.005
		.098	.021			.118	.044
		.078	.058			.100	.094
		.038	.073			.048	.111
		0	.075			0	.112
5	0.240	0	0.102	7	0.320	0	0.119
		−.046	.101			−.050	.118
		−.094	.085			−.104	.102
		−.113	.038			−.122	.048
		−.115	−.009			−.122	−.002
		−.113	−.056			−.122	−.053
		−.094	−.103			−.104	−.107
		−.046	−.119			−.050	−.123
		0	−.120			0	−.124
		.046	−.119			.050	−.123
		.094	−.103			.104	−.107
		.113	−.056			.122	−.053
		.115	−.009			.122	−.002
		.113	.038			.122	.048
		.094	.085			.104	.102
		.046	.101			.050	.118
		0	.102			0	.119

16

Table B2. Continued

(a) Continued

Strip 8 (x = 0.400)

y	z
0	0.125
−.052	.125
−.109	.109
−.125	.052
−.125	0
−.125	−.052
−.109	−.109
−.052	−.125
0	−.125
.052	−.125
.109	−.109
.125	−.052
.125	0
.125	.052
.109	.109
.052	.125
0	.125

Strip 9 (x = 0.450)

y	z
−0.069	0.124
−.089	.120
−.109	.109
−.125	.052
−.125	0
−.125	−.052
−.109	−.109
−.052	−.125
0	−.125
.052	−.125
.109	−.109
.125	−.052
.125	0
.125	.052
.125	.109
.109	.120
.089	.124
.069	

Strip 10 (x = 0.560)

y	z
−0.092	0.119
−.109	.109
−.117	.097
−.125	.052
−.125	0
−.125	−.052
−.109	−.109
−.052	−.125
0	−.125
.052	−.125
.109	−.109
.125	−.052
.125	0
.125	.052
.117	.097
.109	.109
.092	.119

Strip 11 (x = 0.800)

y	z
−0.100	0.115
−.109	.109
−.117	.097
−.125	.052
−.125	0
−.125	−.052
−.109	−.109
−.052	−.125
0	−.125
.052	−.125
.109	−.109
.125	−.052
.125	0
.125	.052
.117	.097
.109	.109
.100	.115

Strip 12 (x = 0.960)

y	z
−0.068	0.120
−.084	.111
−.100	.103
−.115	.051
−.116	.004
−.115	−.044
−.100	−.096
−.048	−.112
0	−.112
.048	−.112
.100	−.096
.115	−.044
.116	.004
.115	.051
.100	.103
.084	.111
.068	.120

Strip 13 (x = 1.018)

y	z
0	0.116
−.046	.116
−.095	.100
−.110	.051
−.111	.006
−.110	−.040
−.095	−.089
−.046	−.105
0	−.105
.046	−.105
.095	−.089
.110	−.040
.111	.006
.110	.051
.095	.100
.046	.116
0	.116

Strip 14 (x = 1.280)

y	z
0	0.099
−.034	.098
−.068	.085
−.081	.051
−.082	.017
−.081	−.016
−.068	−.050
−.034	−.064
0	−.064
.034	−.064
.068	−.050
.081	−.016
.082	.017
.081	.051
.068	.085
.034	.098
0	.099

Strip 15 (x = 1.480)

y	z
0	0.085
−.024	.084
−.047	.073
−.057	.050
−.058	.027
−.057	.003
−.047	−.020
−.024	−.030
0	−.031
.024	−.030
.047	−.020
.057	.003
.058	.027
.057	.050
.047	.073
.024	.084
0	.085

Table B2. Concluded

(a) Concluded

Strip	x	y	z
16	1.720	0	0.070
		−.013	.069
		−.026	.062
		−.033	.050
		−.034	.036
		−.033	.023
		−.026	.011
		−.013	.004
		0	.002
		.013	.004
		.026	.011
		.033	.023
		.034	.036
		.033	.050
		.026	.062
		.013	.069
		0	.070
17	1.900	0	0.065
		−.010	.063
		−.018	.058
		−.023	.050
		−.025	.040
		−.023	.030
		−.018	.022
		−.010	.017
		0	.015
		.010	.017
		.018	.022
		.023	.030
		.025	.040
		.023	.050
		.018	.058
		.010	.063
		0	.065
18	1.960	0	0.060
		−.008	.058
		−.014	.054
		−.018	.048
		−.020	.040
		−.018	.032
		−.014	.026
		−.008	.022
		0	.020
			.022
			.026
			.032
			.040
			.048
			.054
			.058
			.060
19	2.000	0	0.040

(b) Element 2

Strip	x	y	z
0	0.400	0	0.125
1	0.450	0.069	0.124
		.069	.153
		.055	.180
		.025	.184
		0	.184
		−.025	.184
		−.055	.180
		−.069	.153
		−.069	.124
2	0.560	0.092	0.119
		.092	.163
		.073	.198
		.033	.204
		0	.204
		−.033	.204
		−.073	.198
		−.092	.163
		−.092	.119
3	0.800	0.100	0.115
		.099	.166
		.080	.205
		.036	.211
		0	.211
		−.036	.211
		−.080	.205
		−.099	.166
		−.100	.115
4	0.960	0.068	0.124
		.068	.148
		.054	.174
		.024	.178
		0	.178
		−.024	.178
		−.054	.174
		−.068	.148
		−.068	.124
5	1.018	0	0.116

18

Table B3. ROBIN Fuselage-Nacelle-Hub Geometry

(a) Element 1

Strip 0 — x = 0

y	z
0	−0.080

Strip 1 — x = 0.040

y	z
0	−0.003
−.019	−.005
−.037	−.013
−.051	−.029
−.054	−.050
−.051	−.071
−.037	−.087
−.019	−.095
0	−.097
.019	−.095
.037	−.087
.051	−.071
.054	−.050
.051	−.029
.037	−.013
.019	−.005
0	−.003

Strip 2 — x = 0.080

y	z
0	0.031
−.027	.029
−.054	.018
−.071	−.007
−.075	−.037
−.071	−.066
−.054	−.091
−.027	−.102
0	−.104
.027	−.102
.054	−.091
.071	−.066
.075	−.037
.071	−.007
.054	.018
.027	.029
0	.031

Strip 3 — x = 0.120

y	z
0	0.055
−.033	.054
−.067	.040
−.086	.009
−.089	−.027
−.086	−.063
−.067	−.095
−.033	−.108
0	−.110
.033	−.108
.067	−.095
.086	−.063
.089	−.027
.086	.009
.067	.040
.033	.054
0	.055

Strip 4 — x = 0.160

y	z
0	0.075
−.038	.073
−.078	.058
−.098	.021
−.100	−.020
−.098	−.060
−.078	−.098
−.038	−.113
0	−.114
.038	−.113
.078	−.098
.098	−.060
.100	−.020
.098	.021
.078	.058
.038	.073
0	.075

Strip 5 — x = 0.240

y	z
0	0.102
−.046	.101
−.094	.085
−.113	.038
−.115	−.009
−.113	−.056
−.094	−.103
−.046	−.119
0	−.120
.046	−.119
.094	−.103
.113	−.056
.115	−.009
.113	.038
.094	.085
.046	.101
0	.102

Strip 6 — x = 0.280

y	z
0	0.112
−.048	.111
−.100	.094
−.118	.044
−.119	−.005
−.118	−.054
−.100	−.105
−.048	−.121
0	−.122
.048	−.121
.100	−.105
.118	−.054
.119	−.005
.118	.044
.100	.094
.048	.111
0	.112

Strip 7 — x = 0.320

y	z
0	0.119
−.050	.118
−.104	.102
−.122	.048
−.122	−.002
−.122	−.053
−.104	−.107
−.050	−.123
0	−.124
.050	−.123
.104	−.107
.122	−.053
.122	−.002
.122	.048
.104	.102
.050	.118
0	.119

19

Table B3. Continued

(a) Continued

Strip	x	y	z	Strip	x	y	z
8	0.400	0	0.125	9	0.450	-0.069	0.124
		-.052	.125			-.089	.120
		-.109	.109			-.109	.109
		-.125	.052			-.125	.052
		-.125	0			-.125	0
		-.125	-.052			-.125	-.052
		-.109	-.109			-.109	-.109
		-.052	-.125			-.052	-.125
		0	-.125			0	-.125
		.052	-.125			.052	-.125
		.109	-.109			.109	-.109
		.125	-.052			.125	-.052
		.125	0			.125	0
		.125	.052			.125	.052
		.109	.109			.109	.109
		.052	.125			.089	.120
		0	.125			.069	.124

Strip	x	y	z	Strip	x	y	z
10	0.560	-0.092	0.119	11	0.639	-0.098	0.116
		-.109	.109			-.109	.109
		-.117	.097			-.117	.097
		-.125	.052			-.125	.052
		-.125	0			-.125	0
		-.125	-.052			-.125	-.052
		-.109	-.109			-.109	-.109
		-.052	-.125			-.052	-.125
		0	-.125			0	-.125
		.052	-.125			.052	-.125
		.109	-.109			.109	-.109
		.125	-.052			.125	-.052
		.125	0			.125	0
		.125	.052			.125	.052
		.117	.097			.117	.097
		.109	.109			.109	.109
		.092	.119			.098	.116

Strip	x	y	z	Strip	x	y	z
12	0.739	-0.100	0.115	13	0.800	-0.100	0.115
		-.109	.109			-.109	.109
		-.117	.097			-.117	.097
		-.125	.052			-.125	.052
		-.125	0			-.125	0
		-.125	-.052			-.125	-.052
		-.109	-.109			-.109	-.109
		-.052	-.125			-.052	-.125
		0	-.125			0	-.125
		.052	-.125			.052	-.125
		.109	-.109			.109	-.109
		.125	-.052			.125	-.052
		.125	0			.125	0
		.125	.052			.125	.052
		.117	.097			.117	.097
		.109	.109			.109	.109
		.100	.115			.100	.115

Strip	x	y	z	Strip	x	y	z
14	0.960	-0.068	0.120	15	1.018	0	0.116
		-.084	.111			-.046	.116
		-.100	.103			-.095	.100
		-.115	.051			-.110	.051
		-.116	.004			-.111	.006
		-.115	-.044			-.110	-.040
		-.100	-.096			-.095	-.089
		-.048	-.112			-.046	-.105
		0	-.112			0	-.105
		.048	-.112			.046	-.105
		.100	-.096			.095	-.089
		.115	-.044			.110	-.040
		.116	.004			.111	.006
		.115	.051			.110	.051
		.100	.103			.095	.100
		.084	.111			.046	.116
		.068	.120			0	.116

20

Table B3. Continued

(a) Concluded

Strip	x	y	z	Strip	x	y	z
20	1.960	0	0.060	21	2.000	0	0.040
		−.008	.058				
		−.014	.054				
		−.018	.048				
		−.020	.040				
		−.018	.032				
		−.014	.026				
		−.008	.022				
		0	.020				
		.008	.022				
		.014	.026				
		.018	.032				
		.020	.040				
		.018	.048				
		.014	.054				
		.008	.058				
		0	.060				

Strip	x	y	z	Strip	x	y	z
16	1.280	0	0.099	18	1.720	0	0.070
		−.034	.098			−.013	.069
		−.068	.085			−.026	.062
		−.081	.051			−.033	.050
		−.082	.017			−.034	.036
		−.081	−.016			−.033	.023
		−.068	−.050			−.026	.011
		−.034	−.064			−.013	.004
		0	−.064			0	.002
		.034	−.064			.013	.004
		.068	−.050			.026	.011
		.081	−.016			.033	.023
		.082	.017			.034	.036
		.081	.051			.033	.050
		.068	.085			.026	.062
		.034	.098			.013	.069
		0	.099			0	.070
17	1.480	0	0.085	19	1.900	0	0.065
		−.024	.084			−.010	.063
		−.047	.073			−.018	.058
		−.057	.050			−.023	.050
		−.058	.027			−.025	.040
		−.057	.003			−.023	.030
		−.047	−.020			−.018	.022
		−.024	−.030			−.010	.017
		0	−.031			0	.015
		.024	−.030			.010	.017
		.047	−.020			.018	.022
		.057	.003			.023	.030
		.058	.027			.025	.040
		.057	.050			.023	.050
		.047	.073			.018	.058
		.024	.084			.010	.063
		0	.085			0	.065

Table B3. Continued

(b) Element 2

Strip	x	y	z		Strip	x	y	z
0	0.400	0	0.125		5	0.739	0.100	0.115
	→	→	→			→	.099	.166
							.080	.205
							.036	.210
							0	.210
1	0.450	0.069	0.124		6	0.800	0.100	0.115
	→	.069	.153			→	.099	.166
		.055	.180				.080	.205
		.025	.184				.036	.211
		0	.184				0	.211
2	0.560	0.092	0.119		7	0.960	0.068	0.120
	→	.092	.163			→	.068	.148
		.073	.198				.054	.174
		.033	.204				.024	.178
		0	.204				0	.178
3	0.639	0.098	0.116		8	1.018	0	0.116
	→	.097	.165			→	→	→
		.078	.203					
		.035	.208					
		0	.208					
4	0.689	0.099	0.116					
	→	.099	.166					
		.079	.204					
		.065	.210					
		.050	.210					

(c) Element 3

Strip	x	y	z		Strip	x	y	z
0	0.400	0	0.125		5	0.739	0	0.210
	→	→	→			→	−.036	.210
							−.080	.205
							−.099	.166
							−.100	.115
1	0.450	0	0.184		6	0.800	0	0.211
	→	−.025	.184			→	−.036	.211
		−.055	.180				−.080	.205
		−.069	.153				−.099	.166
		−.069	.124				−.100	.115
2	0.560	0	0.204		7	0.960	0	0.178
	→	−.033	.204			→	−.024	.178
		−.073	.198				−.054	.174
		−.092	.163				−.068	.148
		−.092	.119				−.068	.120
3	0.639	0	0.208		8	1.018	0	0.116
	→	−.035	.208			→	→	→
		−.078	.203					
		−.097	.165					
		−.098	.116					
4	0.689	−.050	0.210					
	→	−.065	.210					
		−.079	.204					
		−.099	.166					
		−.099	.116					

Table B3. Concluded

(d) Element 4

Strip	x	y	z	Strip	x	y	z
0	0.639	0	0.208	2	0.663	0	0.232
	.651	−.013	.208		.664	−.010	.232
	.664	−.025	.209		.670	−.018	.232
	.677	−.038	.209		.678	−.023	.233
	.689	−.050	.210		.688	−.025	.233
	.701	−.038	.210		.697	−.023	.233
	.714	−.025	.210		.705	−.018	.234
	.726	−.013	.210		.711	−.010	.234
	.739	0	.210		.713	0	.234
	.726	.013	.210		.711	.010	.234
	.714	.025	.210		.705	.018	.234
	.701	.038	.210		.697	.023	.233
	.689	.050	.210		.688	.025	.233
	.677	.038	.209		.678	.023	.233
	.664	.025	.209		.670	.018	.232
	.651	.013	.208		.664	.010	.232
	.639	0	.208		.663	0	.232
1	0.663	0	0.214	3	0.661	0	0.265
	.665	−.010	.214		.663	−.010	.265
	.671	−.018	.214		.669	−.018	.265
	.679	−.023	.215		.677	−.023	.266
	.688	−.025	.215		.686	−.025	.266
	.698	−.023	.215		.696	−.023	.266
	.706	−.018	.216		.704	−.018	.267
	.711	−.010	.216		.710	−.010	.267
	.713	0	.216		.711	0	.267
	.711	.010	.216		.710	.010	.267
	.706	.018	.216		.704	.018	.267
	.698	.023	.215		.696	.023	.266
	.688	.025	.215		.686	.025	.266
	.679	.023	.215		.677	.023	.266
	.671	.018	.214		.669	.018	.265
	.665	.010	.214		.663	.010	.265
	.663	0	.214		.661	0	.265

Strip	x	y	z	Strip	x	y	z
4	0.553	0	0.275	6	0.683	0	0.356
	.563	−.051	.276		→	→	→
	.592	−.094	.277				
	.635	−.123	.278				
	.686	−.133	.280				
	.737	−.123	.282				
	.780	−.094	.283				
	.809	−.051	.284				
	.819	0	.285				
	.809	.051	.284				
	.780	.094	.283				
	.737	.123	.282				
	.686	.133	.280				
	.635	.123	.278				
	.592	.094	.277				
	.563	.051	.276				
	.553	0	.275				
5	0.551	0	0.325				
	.561	−.051	.326				
	.590	−.094	.327				
	.633	−.123	.328				
	.684	−.133	.330				
	.735	−.123	.332				
	.778	−.094	.333				
	.807	−.051	.334				
	.817	0	.335				
	.807	.051	.334				
	.778	.094	.333				
	.735	.123	.332				
	.684	.133	.330				
	.633	.123	.328				
	.590	.094	.327				
	.561	.051	.326				
	.551	0	.325				

Appendix C

Analysis of Measurement Accuracy

Measurement accuracy in both free-stream velocity and laser velocimeter velocities will be estimated for the particular case of velocity measurements over a helicopter fuselage model in the Langley 14- by 22-Foot Subsonic Tunnel. The perturbation velocity measurements shown here have an estimated error of less than 2.5 percent in the u-component and less than 1.8 percent in the w-component.

Symbols

The symbols used in this appendix are given as follows:

C	tunnel flow correction constant
P_I	indicated pressure, psf
P_T	total or stagnation pressure, psf
P_V	vapor pressure, psf
Q	dynamic pressure, psf
Q_I	indicated dynamic pressure, psf
r	radial distance from hub center
r_m	rotor radius of specific rotor blade set
T_{dew}	dew point, °F
T_R	ambient temperature, °R
U	downstream component of laser-measured velocity, fps
U_P	laser-measured downstream velocity, fps
u	tangential velocity perturbation, fps
u_P	downstream velocity perturbation, fps
V_∞	tunnel free-stream velocity, fps
V_I	tunnel indicated velocity, fps
ΔV	difference velocity (see subsequent text), fps
W	vertical component of laser-measured velocity, fps
w	normal velocity perturbation, fps
α	tip path plane angle of attack
γ	gas constant, 1.4
ρ	fluid density, slugs/ft^3
σ_U	error in U velocity, fps
σ_u	error in u velocity, fps
σ_{V_∞}	error in V_∞ velocity, fps
σ_W	error in W velocity, fps
σ_w	error in w velocity, fps
ψ	rotor azimuth angle, deg

Tunnel Velocity Accuracy

There are several component measurements that affect the calculation of tunnel velocity. The relation used in determining velocity V is

$$V = \sqrt{\frac{2Q}{\rho}} \qquad (C1)$$

where

$$Q = CQ_I \qquad (C2)$$

Here, Q_I is the indicated dynamic pressure and C is an empirical constant, ranging from 1.1266 to 1.1952 and calibrated for each specific wall-floor-suction configuration of the tunnel. The indicated dynamic pressure is measured by a digital pressure gauge with a stated instrument accuracy of ± 0.04 percent of full scale. The instrument used during this test had a full-scale pressure of 200 kPa.

The density ρ is determined from measurement of the temperature, dew point, and total pressure:

$$\rho = \frac{P_T - 0.3789 P_V}{1718.0 T_R} \left(\frac{P_I}{P_T} \right)^{1/\gamma} \qquad (C3)$$

Vapor pressure P_V is found from a simple quadratic in dew point:

$$P_V = 2.80288 + 0.0954685 T_{\text{dew}} + 0.0070509 T_{\text{dew}}^2 \qquad (C4)$$

Ambient temperature T_R (in degrees Rankine) and dew point are read by an electronic dew point hygrometer with a stated accuracy of ± 0.54°F. The total pressure is measured by a digital pressure gauge similar to the dynamic pressure sensor, but with a full-scale range of 0 to 110 kPa.

An estimate of the velocity measurement accuracy can be conducted using several methods. At any given condition, the errors producing the most positive change in velocity can be used to obtain a high estimate, and the errors producing the most negative change in velocity can be used to obtain a low estimate. This type of analysis is a "worst case" method and is not a good estimate of the likely error in the tunnel velocity. A better estimate can be obtained by perturbing each of the error sources separately, finding the high and low velocity perturbations due to each of the error sources, and using the square

root of the sum of the squares of the high perturbations for the high estimate, and likewise for the low estimate.

At the test condition for the helicopter fuselage the values recorded on the static data system will be used for this error estimate. Four separate instrument errors contribute to the errors in dynamic pressure and velocity. A contributing factor to the velocity error is the computation of density. In table C1, the nominal instrument reading and its maximum error are tabulated against the estimates of high- and low-error values resulting from the instrument error using the data reduction procedure in the static data system.

Table C1 shows that the accuracy of the indicated tunnel velocity is principally due to the accuracy of the dynamic-pressure indicating instrument.

Laser Velocimeter Accuracy

The errors in the laser velocimeter measurements are summarized in table C2. These error calculations are based on the development of system measurement precision in references C1 and C2. The main sources of error in these measurements are due to the crossbeam-angle measurement and the clock synchronization and quantization in the signal processor.

The crossbeam-angle error reflects the ability to accurately measure the angle between the two crossed laser beams, since the measured velocity is proportional to the frequency divided by the sine of the angle. The clock synchronization and quantization errors occur in the signal processor as a result of the clock speed and integer nature of the counter.

Other errors, such as time jitter, velocity bias, Bragg bias, and velocity gradient are negligible because of the improvements in the signal processing equipment and the method of data processing over that used in reference C1. The expansion of the laser beams was not measured during the experimental program, so the error induced by diverging fringes in the sample volume is not known. The error introduced by the ability of the seed particle to faithfully follow the flow is dependent upon the size of the particle and the accelerations in the flow. It was found that for this study, the particle lag error is negligible.

The bias errors are summed to give the total bias error, and the total random error is found by taking the square root of the sum of the squares of the individual random errors. The total system error is determined by squaring both the bias and the random error, and then taking the square root of the sum of those squares. The resulting total system error is between 1.19- and 1.80-percent velocity.

Effect of Tunnel Velocity Accuracy

The measured velocity data found in table 1 of the basic report have been corrected for suspected inaccuracies in the measured tunnel velocity. The procedure and rationale for this correction follow.

The large discrepancy between the laser-measured velocity and tunnel free-stream velocity at the forward-most portion of the measurement plane did not correlate well with the expected velocity perturbation due to the presence of the fuselage. After estimating the possible error in tunnel velocity (above), it was determined that the discrepancy between laser measurement and tunnel measurement should be corrected in the presented data.

The least velocity perturbation in the field of laser measurements should occur (from potential theory) at the forward-most position in the measurement plane. At this location the two analytical fuselage models predicted similar perturbations approaching the limiting zero-perturbation case. The velocity correction procedure assumed that a correction velocity ΔV existed that could be defined as the difference between the actual tunnel velocity V_∞ and the indicated tunnel velocity V_I:

$$V_\infty = V_I + \Delta V \qquad (C5)$$

At the forward-most laser measurement, the value measured is assumed to be the sum of the free-stream velocity V_∞ and a perturbation velocity u_P because of the presence of the fuselage:

$$U_P = V_\infty + u_P \qquad (C6)$$

Dividing by the free-stream velocity V_∞ and assuming that the perturbation due to the fuselage is given accurately by the source-panel model, the correction velocity can now be found as

$$\Delta V = \frac{U_P}{1 + (u_P/V_\infty)} - V_I \qquad (C7)$$

The correction velocity was found to be -3.89 fps.

This correction was applied to the tunnel indicated velocity at each measurement location. Table C3 shows the uncorrected or indicated (I) and corrected (C) free-stream velocities and the percent of change in velocity ΔV_∞. The change is about one-half the accuracy computed above.

To demonstrate the effect of this correction, figure C1 shows the differences between the corrected and original velocity perturbations. Figure C1(a) displays the data with the tunnel indicated velocity used as the free-stream velocity, whereas figure C1(b)

displays the data with the free-stream velocity corrected based on the laser velocimeter measurement.

Uncertainty in Presented Perturbation Velocities

To determine the resulting uncertainty in the presented perturbation velocities u and w, the method of Taylor expansion from reference C3 is used. The velocities are computed as

$$u = (U - V_\infty) \cos \alpha + W \sin \alpha \qquad (C8)$$

$$w = W \cos \alpha - (U - V_\infty) \sin \alpha \qquad (C9)$$

The u perturbation velocity can be represented as

$$u = f(U, V_\infty, W) \qquad (C10)$$

This function f can be expanded in a Taylor series:

$$u + \sigma_u = u + \frac{\partial u}{\partial U}\sigma_U + \frac{\partial u}{\partial V_\infty}\sigma_{V_\infty} + \frac{\partial u}{\partial W}\sigma_W \qquad (C11)$$

Assuming independence of the variables U, V_∞, and W, the square of the error σ_u is

$$\sigma_u^2 = \cos^2 \alpha\, \sigma_U^2 + \cos^2 \alpha\, \sigma_{V_\infty}^2 + \sin^2 \alpha\, \sigma_W^2 \qquad (C12)$$

If $\alpha = -3.0°$, then σ_U, σ_{V_∞}, and σ_W are equal to 1.8 percent; the resulting σ_u is 2.5 percent. Similarly, the w perturbation-velocity component error σ_w is computed to be 1.8 percent.

References

C1. Young, Warren H., Jr.; Meyers, James F.; and Hepner, Timothy E.: *Laser Velocimeter Systems Analysis Applied to a Flow Survey Above a Stalled Wing.* NASA TN D-8408, 1977.

C2. Dring, R. P.: Sizing Criteria for Laser Anemometry Particles. Trans. ASME, *J. Fluids Eng.*, vol. 104, Mar. 1982, pp. 15-17.

C3. *Instruments and Apparatus, Part 1—Measurement Uncertainty. Supplement to ASME Performance Test Codes.* ANSI/ASME PTC 19.1-1985. American Soc. of Mechanical Engineers, c.1986.

Table C1. Potential Errors in Tunnel Flow Parameters

Instrument	Nominal	Error	Q, percent	Velocity, percent	Density, percent
Q_I	10.0 psf	1.670 psf	±16.7	+8.06 to −8.76	±0.064
P_T	2137 psf	0.919 psf		±0.022	±0.043
T_{dew}	57.31°F	0.540°F		±0.004	±0.009
T_R	540.0°R	0.540°R		±0.050	±0.100
Cumulative errors			±16.7	+8.06 to −8.76	±0.127

Table C2. Potential Errors in Laser Velocimeter Measurements[a]

Error source	Bias error, percent	Random error, percent
Crossbeam angle measurement	±0.81	N/A
Diverging fringes	N/M	N/M
Time jitter	N/A	N/A
Clock synchronization	0.56	±0.56
Quantization	N/M	±1.02
Velocity bias	Negligible	Negligible
Bragg bias	Negligible	Negligible
Velocity gradient	Negligible	Negligible
Particle lag	Negligible	Negligible
Total errors	−0.25 to 1.37	±1.164

[a]N/A: not applicable; N/M: not measured; Negligible: less than 0.001 percent.

Table C3. Effect of Tunnel Velocity Correction[a]

ψ, deg	r/r_m	$V_{\infty,I}$, fps	$V_{\infty,C}$, fps	ΔV_∞, percent
0	0.20	93.765	89.875	4.15
	.50	94.300	90.410	4.13
	.70	93.778	89.888	4.15
	.82	93.768	89.878	4.15
	.90	93.771	89.881	4.15
	1.02	93.770	89.880	4.15
180	0.20	94.479	90.589	4.12
	.50	94.452	90.562	4.12
	.70	94.426	90.536	4.12
	.82	93.794	89.904	4.15
	.90	94.336	90.476	4.12
	1.02	93.817	89.927	4.15

[a]Subscript I: indicated; subscript C: corrected.
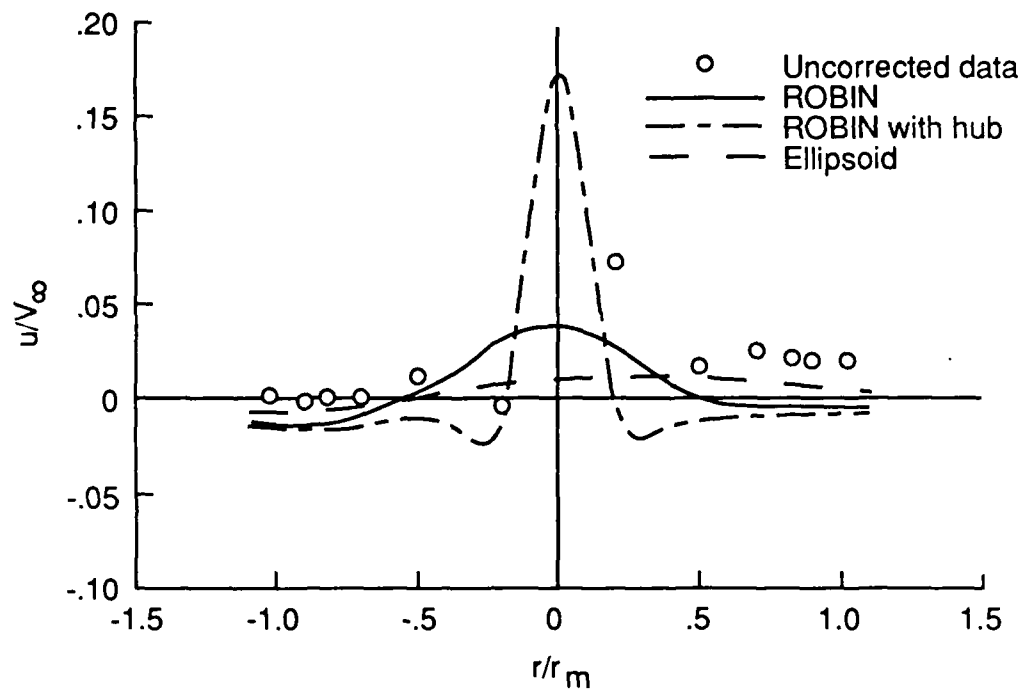
(a) Tunnel indicated velocity.
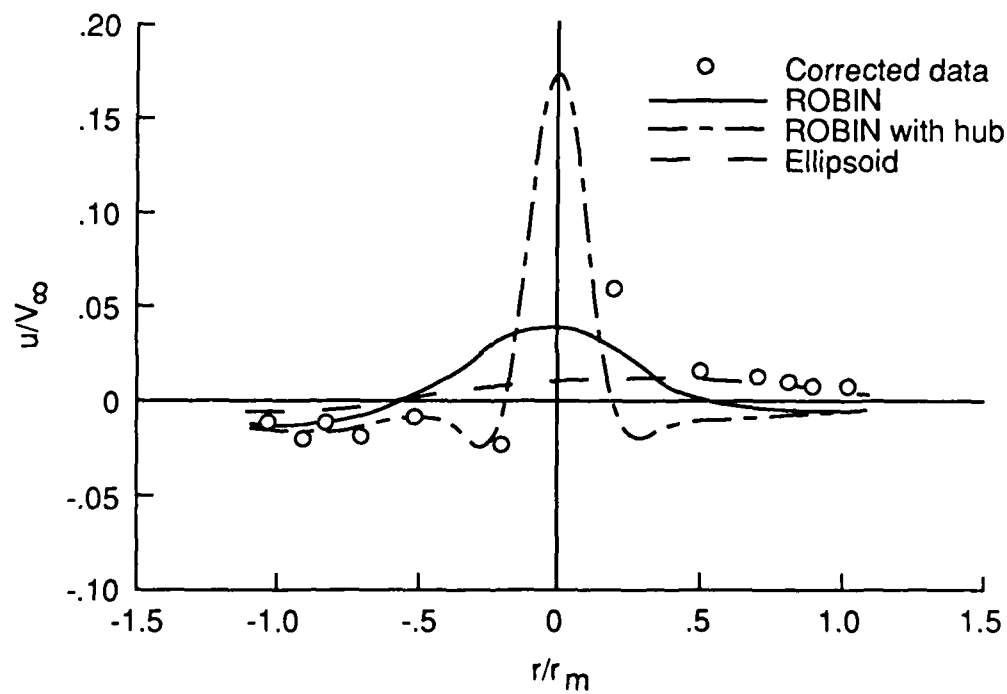
(b) Corrected free-stream velocity.

Figure C1. Velocity perturbations over fuselage centerline.

References

1. Davis, Sanford S.; and Chang, I-Chung: The Critical Role of Computational Fluid Dynamics in Rotary-Wing Aerodynamics. AIAA-86-0336, Jan. 1986.

2. Wilson, John C.; and Mineck, Raymond E.: *Wind-Tunnel Investigation of Helicopter-Rotor Wake Effects on Three Helicopter Fuselage Models.* NASA TM X-3185, 1975.

3. Sheridan, Philip F.: *Interactional Aerodynamics of the Single Rotor Helicopter Configuration. Volume I—Final Report.* USARTL-TR-78-23A, U.S. Army, Sept. 1978. (Available from DTIC as AD A060 389.)

4. Freeman, Carl E.; and Mineck, Raymond E.: *Fuselage Surface Pressure Measurements of a Helicopter Wind-Tunnel Model With a 3.15-Meter Diameter Single Rotor.* NASA TM-80051, 1979.

5. Keys, C. N.: *Rotary-Wing Aerodynamics. Volume II: Performance Prediction of Helicopters.* Dover Publ., Inc., 1984.

6. Betzina, Mark D.; and Shinoda, Patrick: *Aerodynamic Interactions Between a 1/6-Scale Helicopter Rotor and a Body of Revolution.* NASA TM-84247, USAAVRADCOM TR-82-A-6, 1982.

7. Betzina, Mark D.; Smith, Charles A.; and Shinoda, Patrick: *Rotor/Body Aerodynamic Interactions.* NASA TM-85844, USAAVRADCOM TR-83-A-12, 1983.

8. Komerath, N. M.; McMahon, H. M.; and Hubbartt, J. E.: Aerodynamic Interactions Between a Rotor and Airframe in Forward Flight. AIAA-85-1606, July 1985.

9. Brand, A. G.; Komerath, N. M.; and McMahon, H. M.: *Wind Tunnel Data From a Rotor Wake/Airframe Interaction Study.* ARO 19364.18-EG-RW, U.S. Army, July 1986. (Available from DTIC as AD A171 333.)

10. Crimi, Peter; and Trenka, Andrew R.: *Theoretical Prediction of the Flow in the Wake of a Helicopter Rotor. Addendum—Effects Due to a Fuselage in a Constant, Nonuniform Flow.* BB-1994-S-3 (Contract No. DA30-069-AMC-645(R)), Cornell Aeronautical Lab., Inc., Aug. 1966. (Available from DTIC as AD 637 872.)

11. Huber, H.; and Polz, G.: Studies on Blade-to-Blade and Rotor-Fuselage-Tail Interferences. *Prediction of Aerodynamic Loads on Rotorcraft.* AGARD-CP-334, Sept. 1982, pp. 9-1—9-16.

12. Freeman, Carl Edward: *Calculation of Helicopter Fuselage Surface Pressures in the Presence of a Rotor Wake and Correlation With Experimental Data.* M.S. Thesis, George Washington Univ., Aug. 1979.

13. Freeman, Carl E.: *Development and Validation of a Combined Rotor-Fuselage Induced Flow-Field Computational Method.* NASA TP-1656, AVRADCOM TR 80-B-3, 1980.

14. Polz, G. (Leo Kanner Assoc., transl.): *The Calculation of Separated Flow at Helicopter Bodies.* NASA TM-76715, 1982.

15. Johnson, W.; and Yamauchi, G. K.: *Aplications of an Analysis of Axisymmetric Body Effects on Rotor Performance and Loads. Tenth European Rotorcraft Forum, Volume I,* 1984, Paper Nr.: 3.

16. Brand, Albert G.; Liou, Shiuh-Guang; Komerath, Narayanan M.; and McMahon, Howard M.: Rotor-Airframe Aerodynamic Interaction Phenomena. *Proceedings of the 2nd International Conference on Rotorcraft Basic Research,* Univ. of Maryland and American Helicopter Soc., Feb. 1988.

17. Ryan, Juliette; Falempin, Grégoire; and Hiệp, Lê Thiên: *Rotor Plane Velocities Induced by a Helicopter Fuselage.* ONERA T.P. No. 1988-22, 1988.

18. Berry, J. D.; Hoad, D. R.; Elliott, J. W.; and Althoff, S. L.: *Helicopter Rotor Induced Velocities Theory and Experiment.* Paper presented at the AHS Specialists Meeting on Aerodynamics and Aeroacoustics (Arlington, Texas), Feb. 25-27, 1987.

19. Elliott, Joe W.; Althoff, Susan L.; and Sailey, Richard H.: *Inflow Measurement Made With a Laser Velocimeter on a Helicopter Model in Forward Flight. Volume I—Rectangular Planform Blades at an Advance Ratio of 0.15.* NASA TM-100541, AVSCOM TM-88-B-004, 1988.

20. Elliott, Joe W.; Althoff, Susan L.; and Sailey, Richard H.: *Inflow Measurement Made With a Laser Velocimeter on a Helicopter Model in Forward Flight. Volume II—Rectangular Planform Blades at an Advance Ratio of 0.23.* NASA TM-100542, AVSCOM TM-88-B-005, 1988.

21. Elliott, Joe W.; Althoff, Susan L.; and Sailey, Richard H.: *Inflow Measurement Made With a Laser Velocimeter on a Helicopter Model in Forward Flight. Volume III—Rectangular Planform Blades at an Advance Ratio of 0.30.* NASA TM-100543, AVSCOM TM-88-B-006, 1988.

22. Elliott, Joe W.; Althoff, Susan L.; and Sailey, Richard H.: *Inflow Measurement Made With a Laser Velocimeter on a Helicopter Model in Forward Flight. Volume IV—Tapered Planform Blades at an Advance Ratio of 0.15.* NASA TM-100544, AVSCOM TM-88-B-007, 1988.

23. Elliott, Joe W.; Althoff, Susan L.; and Sailey, Richard H.: *Inflow Measurement Made With a Laser Velocimeter on a Helicopter Model in Forward Flight. Volume V—Tapered Planform Blades at an Advance Ratio of 0.23.* NASA TM-100545, AVSCOM TM-88-B-008, 1988.

24. Hoad, Danny R.; Althoff, Susan L.; and Elliott, Joe W.: Rotor Inflow Variability With Advance Ratio. *44th Annual Forum Proceedings, American Helicopter Soc.,* c.1988, pp. 57-72.

25. Elliott, Joe W.; Althoff, Susan L.; Sellers, William L., III; and Nichols, Cecil E., Jr.: Inflow Velocity Measurements Made on a Helicopter Rotor Using a Two-Component Laser Velocimeter. AIAA-87-1321, June 1987.

26. Hess, John L.; and Smith, A. M. O.: *Calculation of Non-Lifting Potential Flow About Arbitrary Three-Dimensional Bodies.* Rep. No. E.S. 40622 (Contract No. Nonr 2722(00)), Douglas Aircraft Co., Inc., Mar. 15, 1962.

27. Hess, J. L.; and Smith, A. M. O.: Calculation of Potential Flow About Arbitrary Bodies. *Progress in Aeronautical Sciences, Volume 8,* D. Kuchemann, ed., Pergamon Press Inc., c.1967, pp. 1-138.

28. Press, William H.; Flannery, Brian P.; Teukolsky, Saul A.; and Vetterling, William T.: *Numerical Recipes—The Art of Scientific Computing.* Cambridge Univ. Press, c.1986.

29. Wilson, John C.: A General Rotor Model System for Wind-Tunnel Investigations. *J. Aircr.*, vol. 14, no. 7, July 1977, pp. 639–643.

30. Applin, Zachary T.: *Flow Improvements in the Circuit of the Langley 4- by 7-Meter Tunnel.* NASA TM-85662, 1983.

31. Sellers, William L.; and Elliott, Joe W.: Applications of a Laser Velocimeter in the Langley 4- by 7-Meter Tunnel. *Flow Visualization and Laser Velocimetry for Wind Tunnels,* William W. Hunter, Jr., and Jerome T. Foughner, Jr., editors, NASA CP-2243, 1982, pp. 283–293.

32. Elliott, Joe W.; and Nichols, Cecil E.: Seeding Systems for Use With a Laser Velocimeter in Large Scale Wind Tunnels. *Wind Tunnel Seeding Systems for Laser Velocimeters,* William W. Hunter, Jr., and Cecil E. Nichols, Jr., compilers, NASA CP-2393, 1985, p. 93–103.

33. Phelps, Arthur E., III; and Berry, John D.: *Description of the U.S. Army Small-Scale 2-Meter Rotor Test System.* NASA TM-87762, AVSCOM TM 86-B-4, 1987.

Table 1. Measured Induced Velocities of Fuselage

[Corrected values from table C3]

ψ, deg	r/r_m	u/V_∞	σ_u, fps	O_u	w/V_∞	σ_w, fps	O_w	V_∞, fps
0	0.20	0.0594	0.0359	1518	0.0053	0.0093	1190	89.875
	.50	.0158	.0344	1434	−.0199	.0291	1175	90.410
	.70	.0127	.0333	1539	−.0153	.0306	1108	89.888
	.82	.0096	.0326	1469	−.0119	.0313	1065	89.878
	.90	.0075	.0339	1467	−.0114	.0293	981	89.881
	1.02	.0079	.0333	1415	−.0102	.0299	1031	89.880
180	0.20	−0.0239	0.0376	1345	0.0807	0.0324	515	90.589
	.50	−.0086	.0403	611	.0556	.0297	195	90.562
	.70	−.0191	.0430	139				90.536
	.82	−.0124	.0353	1505	.0391	.0293	794	89.904
	.90	−.0211	.0350	1531	.0346	.0284	596	90.476
	1.02	−.0121	.0366	1559	.0270	.0299	695	89.927

Table 2. Test Conditions Described in References 19-23

Reference	r_m/R	α, deg	V_∞, fps
19	0.8470	−3.00	93.0
20	.8470	−3.04	143.2
21	.8470	−4.04	187.1
22	.8125	−3.04	94.1
23	.8125	−3.05	144.0

Table 3. Induced Velocity Perturbations of Basic Fuselage Computed at Inflow Measurement Plane

(a) $r_m/R = 0.8470$; $\alpha = -3.0°$

ψ, deg	r/r_m	u/V_∞	v/V_∞	w/V_∞	ψ, deg	r/r_m	u/V_∞	v/V_∞	w/V_∞
0	0.20	0.027622	−0.000150	−0.027460	180	0.20	0.031654	−0.000208	0.034158
	.40	.006401	−.000129	−.033328		.40	.011556	−.000209	.046595
	.50	.000416	−.000095	−.029066		.50	.003801	−.000172	.045412
	.60	−.002422	−.000058	−.024602		.60	−.002628	−.000128	.042575
	.70	−.003833	−.000044	−.021063		.70	−.008236	−.000097	.037851
	.74	−.004176	−.000036	−.019825		.74	−.010052	−.000087	.035394
	.78	−.004463	−.000030	−.018691		.78	−.011544	−.000078	.032736
	.82	−.004712	−.000024	−.017639		.82	−.012680	−.000070	.029938
	.86	−.004929	−.000020	−.016648		.86	−.013454	−.000063	.027094
	.90	−.005117	−.000016	−.015705		.90	−.013903	−.000057	.024293
	.94	−.005273	−.000013	−.014794		.94	−.014019	−.000051	.021606
	.98	−.005386	−.000007	−.013937		.98	−.013879	−.000045	.019095
	1.02	−.005493	−.000004	−.013107		1.02	−.013538	−.000040	.016793
	1.04	−.005540	−.000002	−.012712		1.04	−.013309	−.000038	.015725
	1.10	−.005625	0	−.011542		1.10	−.012456	−.000032	.012864
30	0.20	0.028703	−0.005137	−0.021882	210	0.20	0.031864	−0.008950	0.026492
	.40	.011359	−.011401	−.023959		.40	.015995	−.018060	.029609
	.50	.006164	−.011676	−.020305		.50	.009949	−.019169	.026436
	.60	.003100	−.011059	−.016651		.60	.005230	−.018872	.022699
	.70	.001272	−.010136	−.013556		.70	.001559	−.017598	.018801
	.74	.000752	−.009742	−.012481		.74	.000378	−.016891	.017259
	.78	.000316	−.009350	−.011494		.78	−.000623	−.016098	.015750
	.82	−.000048	−.008961	−.010586		.82	−.001457	−.015243	.014294
	.86	−.000355	−.008580	−.009753		.86	−.002131	−.014353	.012912
	.90	−.000615	−.008203	−.008980		.90	−.002659	−.013448	.011616
	.94	−.000839	−.007826	−.008258		.94	−.003055	−.012548	.010416
	.98	−.001024	−.007463	−.007601		.98	−.003336	−.011667	.009316
	1.02	−.001182	−.007103	−.006986		1.02	−.003521	−.010819	.008316
	1.04	−.001250	−.006930	−.006701		1.04	−.003582	−.0104Cɟ	.007853
	1.10	−.001411	−.006417	−.005902		1.10	−.003664	−.009247	.006604

Table 3. Continued

(a) Continued

ψ, deg	r/r_m	u/V_∞	v/V_∞	w/V_∞	ψ, deg	r/r_m	u/V_∞	v/V_∞	w/V_∞
60	0.20	0.030362	−0.003487	−0.010684	240	0.20	0.031798	−0.008302	0.012668
	.40	017344	−.007670	−.010557		.40	.019523	−.012185	.010122
	.50	.012860	−.007759	−.008696		.50	.014845	−.011731	.008079
	.60	.009654	−.007263	−.006942		.60	.011230	−.010716	.006351
	.70	.007329	−.006544	−.005491		.70	.008468	−.009519	.004965
	.74	.006591	−.006242	−.004998		.74	.007564	−.009024	.004491
	.78	.005937	−.005940	−.004550		.78	.006757	−.008538	.004062
	.82	.005360	−.005643	−.004144		.82	.006037	−.008059	.003671
	.86	.004848	−.005353	−.003775		.86	.005397	−.007595	.003316
	.90	.004393	−.005072	−.003443		.90	.004827	−.007149	.002996
	.94	.003985	−.004807	−.003144		.94	.004322	−.006722	.002706
	.98	.003623	−.004548	−.002872		.98	.003873	−.006313	.002444
	1.02	.003301	−.004302	−.002626		1.02	.003476	−.005927	.002208
	1.04	.003152	−.004184	−.002512		1.04	.003294	−.005741	.002099
	1.10	.002749	−.003847	−.002202		1.10	.002810	−.005217	.001805
90	0.20	0.031299	0.002389	0.000704	270	0.20	0.031269	−0.002499	0.000506
	.40	.019696	.001763	−.000661		.40	.019667	−.001718	−.000806
	.50	.015395	.001359	−.000740		.50	.015370	−.001298	−.000849
	.60	.012103	.001041	−.000696		.60	.012083	−.000978	−.000771
	.70	.009597	.000815	−.000604		.70	.009580	−.000758	−.000657
	.74	.008770	.000744	−.000565		.74	.008755	−.000690	−.000611
	.78	.008027	.000681	−.000527		.78	.008013	−.000631	−.000566
	.82	.007363	.000625	−.000491		.82	.007350	−.000579	−.000525
	.86	.006759	.000576	−.000456		.86	.006747	−.000532	−.000486
	.90	.006215	.000531	−.000424		.90	.006204	−.000491	−.000450
	.94	.005726	.000490	−.000394		.94	.005715	−.000453	−.000417
	.98	.005282	.000454	−.000367		.98	.005273	−.000419	−.000387
	1.02	.004880	.000421	−.000341		1.02	.004871	−.000389	−.000359
	1.04	.004693	.000406	−.000329		1.04	.004684	−.000375	−.000346
	1.10	.004183	.000364	−.000296		1.10	.004175	−.000336	−.000310

Table 3. Continued

(a) Concluded

ψ, deg	r/r_m	u/V_∞	v/V_∞	w/V_∞	ψ, deg	r/r_m	u/V_∞	v/V_∞	w/V_∞
120	0.20	0.031860	0.008169	0.012908	300	0.20	0.030354	0.003342	−0.010873
	.40	.019553	.012232	.010347		.40	.017321	.007707	−.010721
	.50	.014851	.011809	.008245		.50	.012823	.007828	−.008819
	.60	.011222	.010795	.006468		.60	.009610	.007322	−.007028
	.70	.008455	.009590	.005047		.70	.007287	.006594	−.005544
	.74	.007549	.009090	.004563		.74	.006551	.006286	−.005041
	.78	.006742	.008599	.004124		.78	.005898	.005979	−.004586
	.82	.006022	.008115	.003724		.82	.005323	.005678	−.004174
	.86	.005382	.007647	.003363		.86	.004813	.005384	−.003801
	.90	.004813	.007198	.003038		.90	.004361	.005099	−.003464
	.94	.004307	.006767	.002743		.94	.003956	.004831	−.003162
	.98	.003860	.006355	.002477		.98	.003596	.004570	−.002887
	1.02	.003462	.005965	.002237		1.02	.003275	.004321	−.002639
	1.04	.003281	.005778	.002126		1.04	.003127	.004202	−.002524
	1.10	.002797	.005250	.001828		1.10	.002728	.003862	−.002211
150	0.20	0.031921	0.008669	0.026720	330	0.20	0.028709	0.004903	−0.022038
	.40	.015957	.017969	.029969		.40	.011303	.011321	−.024182
	.50	.009862	.019136	.026724		.50	.006067	.011653	−.020466
	.60	.005140	.018867	.022902		.60	.003003	.011057	−.016757
	.70	.001479	.017604	.018945		.70	.001188	.010134	−.013617
	.74	.000304	.016899	.017386		.74	.000675	.009741	−.012528
	.78	−.000693	.016107	.015861		.78	.000246	.009346	−.011526
	.82	−.001522	.015254	.014392		.82	−.000111	.008959	−.010609
	.86	−.002192	.014365	.012999		.86	−.000409	.008576	−.009764
	.90	−.002716	.013460	.011693		.90	−.000664	.008201	−.008987
	.94	−.003108	.012560	.010484		.94	−.000882	.007822	−.008260
	.98	−.003386	.011679	.009375		.98	−.001062	.007459	−.007599
	1.02	−.003568	.010830	.008368		1.02	−.001215	.007098	−.006983
	1.04	−.003628	.010419	.007901		1.04	−.001279	.006923	−.006696
	1.10	−.003706	.009257	.006644		1.10	−.001436	.006409	−.005896

Table 3. Continued

(b) $r_m/R = 0.8470$; $\alpha = -4.0°$

ψ, deg	r/r_m	u/V_∞	v/V_∞	w/V_∞	ψ, deg	r/r_m	u/V_∞	v/V_∞	w/V_∞
0	0.20	0.028314	−0.000142	−0.024951	180	0.20	0.031126	−0.000211	0.036910
	.40	.007224	−.000119	−.031642		.40	.010669	−.000215	.048646
	.50	.001199	−.000086	−.027701		.50	.002816	−.000178	.047073
	.60	−.001691	−.000050	−.023493		.60	−.003649	−.000133	.043812
	.70	−.003153	−.000037	−.020180		.70	−.009205	−.000100	.038671
	.74	−.003518	−.000029	−.019024		.74	−.010978	−.000090	.036062
	.78	−.003828	−.000023	−.017969		.78	−.012416	−.000081	.033269
	.82	−.004100	−.000018	−.016991		.82	−.013490	−.000073	.030351
	.86	−.004342	−.000014	−.016070		.86	−.014199	−.000065	.027404
	.90	−.004556	−.000010	−.015192		.90	−.014581	−.000059	.024516
	.94	−.004739	−.000008	−.014343		.94	−.014630	−.000053	.021758
	.98	−.004877	−.000002	−.013545		.98	−.014425	−.000047	.019189
	1.02	−.005013	.000001	−.012770		1.02	−.014025	−.000042	.016844
	1.04	−.005075	.000003	−.012402		1.04	−.013767	−.000040	.015757
	1.10	−.005201	.000005	−.011297		1.10	−.012836	−.000033	.012853
30	0.20	0.029263	−0.004164	−0.019674	210	0.20	0.031458	−0.009995	0.028872
	.40	.011935	−.010341	−.022864		.40	.015422	−.019269	.030887
	.50	.006678	−.010725	−.019588		.50	.009367	−.020257	.027277
	.60	.003548	−.010242	−.016206		.60	.004676	−.019777	.023193
	.70	.001657	−.009460	−.013304		.70	.001064	−.018304	.019047
	.74	.001113	−.009121	−.012288		.74	−.000086	−.017522	.017431
	.78	.000654	−.008781	−.011350		.78	−.001054	−.016657	.015862
	.82	.000267	−.008443	−.010486		.82	−.001855	−.015737	.014357
	.86	−.000061	−.008109	−.009688		.86	−.002496	−.014787	.012935
	.90	−.000341	−.007778	−.008946		.90	−.002992	−.013828	.011610
	.94	−.000585	−.007442	−.008248		.94	−.003357	−.012880	.010386
	.98	−.000790	−.007117	−.007611		.98	−.003610	−.011957	.009269
	1.02	−.000967	−.006792	−.007012		1.02	−.003768	−.011072	.008257
	1.04	−.001043	−.006635	−.006733		1.04	−.003816	−.010645	.007789
	1.10	−.001230	−.006166	−.005948		1.10	−.003864	−.009441	.006531

Table 3. Continued

(b) Continued

ψ, deg	r/r_m	u/V_∞	v/V_∞	w/V_∞	ψ, deg	r/r_m	u/V_∞	v/V_∞	w/V_∞
60	0.20	0.030665	−0.002059	−0.008949	240	0.20	0.031628	−0.009782	0.014470
	.40	.017587	−.006489	−.010071		.40	.019320	−.013432	.010641
	.50	.013057	−.006829	−.008502		.50	.014655	−.012715	.008288
	.60	.009812	−.006551	−.006908		.60	.011060	−.011462	.006388
	.70	.007457	−.006008	−.005538		.70	.008323	−.010074	.004915
	.74	.006708	−.005764	−.005064		.74	.007429	−.009515	.004420
	.78	.006044	−.005514	−.004629		.78	.006632	−.008972	.003978
	.82	.005458	−.005264	−.004232		.82	.005922	−.008443	.003578
	.86	.004937	−.005014	−.003870		.86	.005290	−.007934	.003217
	.90	.004474	−.004770	−.003540		.90	.004729	−.007450	.002894
	.94	.004059	−.004537	−.003242		.94	.004232	−.006988	.002603
	.98	.003691	−.004306	−.002970		.98	.003791	−.006550	.002342
	1.02	.003363	−.004086	−.002722		1.02	.003400	−.006137	.002108
	1.04	.003211	−.003978	−.002607		1.04	.003221	−.005940	.002001
	1.10	.002801	−.003672	−.002293		1.10	.002746	−.005384	.001711
90	0.20	0.031366	0.003932	0.002265	270	0.20	0.031325	−0.004038	0.002068
	.40	.019721	.002913	−.000339		.40	.019682	−.002867	−.000481
	.50	.015407	.002229	−.000666		.50	.015374	−.002168	−.000771
	.60	.012107	.001686	−.000739		.60	.012081	−.001624	−.000812
	.70	.009597	.001291	−.000698		.70	.009575	−.001236	−.000748
	.74	.008768	.001166	−.000668		.74	.008748	−.001114	−.000712
	.78	.008025	.001056	−.000635		.78	.008006	−.001007	−.000673
	.82	.007360	.000958	−.000602		.82	.007343	−.000913	−.000635
	.86	.006756	.000872	−.000567		.86	.006740	−.000830	−.000596
	.90	.006211	.000795	−.000534		.90	.006197	−.000756	−.000559
	.94	.005722	.000725	−.000502		.94	.005709	−.000689	−.000524
	.98	.005279	.000664	−.000471		.98	.005267	−.000630	−.000490
	1.02	.004877	.000609	−.000442		1.02	.004865	−.000578	−.000459
	1.04	.004689	.000584	−.000428		1.04	.004679	−.000554	−.000444
	1.10	.004179	.000515	−.000389		1.10	.004170	−.000489	−.000402

Table 3. Continued

(b) Concluded

ψ, deg	r/r_m	u/V_∞	v/V_∞	w/V_∞	ψ, deg	r/r_m	u/V_∞	v/V_∞	w/V_∞
120	0.20	0.031699	0.009650	0.014715	300	0.20	0.030648	0.001919	−0.009132
	.40	.019358	.013484	.010871		.40	.017557	.006526	−.010224
	.50	.014666	.012798	.008457		.50	.013014	.006894	−.008613
	.60	.011057	.011545	.006507		.60	.009765	.006606	−.006984
	.70	.008313	.010147	.004998		.70	.007411	.006053	−.005583
	.74	.007417	.009583	.004493		.74	.006665	.005804	−.005100
	.78	.006620	.009036	.004041		.78	.006002	.005549	−.004658
	.82	.005909	.008502	.003631		.82	.005418	.005294	−.004256
	.86	.005277	.007989	.003265		.86	.004900	.005040	−.003889
	.90	.004716	.007500	.002936		.90	.004440	.004792	−.003556
	.94	.004219	.007035	.002641		.94	.004028	.004556	−.003255
	.98	.003779	.006593	.002375		.98	.003663	.004323	−.002980
	1.02	.003389	.006177	.002137		1.02	.003336	.004100	−.002731
	1.04	.003210	.005978	.002028		1.04	.003185	.003992	−.002615
	1.10	.002735	.005418	.001734		1.10	.002779	.003683	−.002299
150	0.20	0.031521	0.009710	0.029108	330	0.20	0.029264	0.003940	−0.019821
	.40	.015385	.019180	.031260		.40	.011877	.010268	−.023071
	.50	.009278	.020226	.027575		.50	.006579	.010707	−.019734
	.60	.004585	.019773	.023404		.60	.003452	.010242	−.016297
	.70	.000984	.018312	.019197		.70	.001574	.009459	−.013352
	.74	−.000161	.017532	.017564		.74	.001037	.009119	−.012322
	.78	−.001125	.016668	.015978		.78	.000585	.008776	−.011371
	.82	−.001921	.015750	.014459		.82	.000206	.008440	−.010498
	.86	−.002559	.014800	.013026		.86	−.000113	.008104	−.009689
	.90	−.003050	.013842	.011689		.90	−.000388	.007773	−.008942
	.94	−.003412	.012893	.010456		.94	−.000626	.007435	−.008241
	.98	−.003661	.011970	.009331		.98	−.000825	.007110	−.007599
	1.02	−.003816	.011084	.008311		1.02	−.000997	.006784	−.006999
	1.04	−.003863	.010657	.007840		1.04	−.001070	.006625	−.006718
	1.10	−.003906	.009451	.006572		1.10	−.001251	.006155	−.005934

Table 3. Continued

(c) $r_m/R = 0.8125$; $\alpha = -3.0°$

ψ, deg	r/r_m	u/V_∞	v/V_∞	w/V_∞	ψ, deg	r/r_m	u/V_∞	v/V_∞	w/V_∞
0	0.20	0.028476	−0.000149	−0.026583	180	0.20	0.032332	−0.000201	0.033065
	.40	.007763	−.000134	−.033793		.40	.013056	−.000214	.046535
	.50	.001325	−.000102	−.030033		.50	.005217	−.000182	.045818
	.60	−.001926	−.000065	−.025631		.60	−.001117	−.000128	.043412
	.70	−.003532	−.000051	−.022014		.70	−.006771	−.000104	.039418
	.74	−.003923	−.000042	−.020747		.74	−.008711	−.000094	.037276
	.78	−.004239	−.000035	−.019585		.78	−.010386	−.000085	.034863
	.82	−.004507	−.000029	−.018513		.82	−.011756	−.000077	.032281
	.86	−.004740	−.000024	−.017513		.86	−.012795	−.000069	.029585
	.90	−.004946	−.000019	−.016568		.90	−.013503	−.000063	.026857
	.94	−.005124	−.000016	−.015665		.94	−.013914	−.000056	.024175
	.98	−.005273	−.000013	−.014793		.98	−.014019	−.000051	.021601
	1.02	−.005381	−.000008	−.013970		1.02	−.013888	−.000046	.019188
	1.04	−.005434	−.000007	−.013560		1.04	−.013750	−.000043	.018052
	1.10	−.005565	−.000001	−.012413		1.10	−.013113	−.000037	.014952
30	0.20	0.029435	−0.004765	−0.021272	210	0.20	0.032461	−0.008421	0.025863
	.40	.012470	−.011205	−.024446		.40	.017144	−.017684	.029981
	.50	.007013	−.011724	−.021085		.50	.011050	−.019082	.027154
	.60	.003706	−.011240	−.017482		.60	.006279	−.019042	.023629
	.70	.001708	−.010415	−.014380		.70	.002500	−.018045	.019918
	.74	.001135	−.010039	−.013282		.74	.001250	−.017434	.018419
	.78	.000656	−.009661	−.012271		.78	.000158	−.016734	.016944
	.82	.000251	−.009285	−.011338		.82	−.000772	−.015960	.015505
	.86	−.000088	−.008914	−.010479		.86	−.001549	−.015134	.014118
	.90	−.000379	−.008548	−.009685		.90	−.002181	−.014278	.012800
	.94	−.000625	−.008187	−.008948		.94	−.002678	−.013409	.011563
	.98	−.000839	−.007826	−.008256		.98	−.003055	−.012546	.010414
	1.02	−.001018	−.007477	−.007625		1.02	−.003327	−.011701	.009357
	1.04	−.001099	−.007302	−.007323		1.04	−.003428	−.011288	.008863
	1.10	−.001295	−.006797	−.006488		1.10	−.003616	−.010105	.007517

Table 3. Continued

(c) Continued

ψ, deg	r/r_m	u/V_∞	v/V_∞	w/V_∞	ψ, deg	r/r_m	u/V_∞	v/V_∞	w/V_∞
60	0.20	0.030930	−0.003208	−0.010424	240	0.20	0.032301	−0.007959	0.012593
	.40	.018218	−.007554	−.010832		.40	.020397	−.012167	.010479
	.50	.013661	−.007808	−.009079		.50	.015705	−.011888	.008474
	.60	.010350	−.007414	−.007343		.60	.012026	−.010989	.006741
	.70	.007917	−.006758	−.005873		.70	.009180	−.009868	.005330
	.74	.007137	−.006471	−.005366		.74	.008235	−.009397	.004844
	.78	.006450	−.006181	−.004902		.78	.007391	−.008925	.004400
	.82	.005837	−.005890	−.004480		.82	.006633	−.008458	.003994
	.86	.005293	−.005607	−.004096		.86	.005954	−.008001	.003625
	.90	.004809	−.005328	−.003745		.90	.005346	−.007557	.003288
	.94	.004375	−.005060	−.003429		.94	.004804	−.007130	.002983
	.98	.003984	−.004806	−.003143		.98	.004321	−.006721	.002705
	1.02	.003637	−.004558	−.002882		1.02	.003890	−.006329	.002454
	1.04	.003477	−.004438	−.002760		1.04	.003692	−.006140	.002337
	1.10	.003043	−.004096	−.002429		1.10	.003163	−.005604	.002020
90	0.20	0.031800	0.002375	0.000810	270	0.20	0.031759	−0.002486	0.000605
	.40	.020498	.001831	−.000637		.40	.020475	−.001783	−.000793
	.50	.016185	.001433	−.000740		.50	.016160	−.001373	−.000856
	.60	.012827	.001109	−.000713		.60	.012806	−.001046	−.000796
	.70	.010242	.000873	−.000631		.70	.010224	−.000814	−.000689
	.74	.009385	.000797	−.000594		.74	.009368	−.000741	−.000645
	.78	.008611	.000730	−.000557		.78	.008596	−.000678	−.000601
	.82	.007912	.000672	−.000520		.82	.007898	−.000622	−.000559
	.86	.007284	.000619	−.000486		.86	.007272	−.000573	−.000520
	.90	.006712	.000572	−.000453		.90	.006700	−.000529	−.000483
	.94	.006193	.000530	−.000422		.94	.006182	−.000490	−.000449
	.98	.005725	.000490	−.000394		.98	.005714	−.000453	−.000417
	1.02	.005298	.000455	−.000368		1.02	.005289	−.000420	−.000388
	1.04	.005099	.000439	−.000355		1.04	.005090	−.000405	−.000374
	1.10	.004556	.000395	−.000320		1.10	.004548	−.000365	−.000336

Table 3. Continued

(c) Concluded

ψ, deg	r/r_m	u/V_∞	v/V_∞	w/V_∞	ψ, deg	r/r_m	u/V_∞	v/V_∞	w/V_∞
120	0.20	0.032363	0.007815	0.012827	300	0.20	0.030922	0.003053	−0.010609
	.40	.020432	.012198	.010702		.40	.018195	.007585	−.011008
	.50	.015715	.011963	.008652		.50	.013625	.007873	−.009212
	.60	.012020	.011069	.006869		.60	.010306	.007475	−.007439
	.70	.009167	.009941	.005421		.70	.007874	.006811	−.005933
	.74	.008221	.009466	.004923		.74	.007095	.006519	−.005416
	.78	.007376	.008989	.004470		.78	.006409	.006224	−.004944
	.82	.006618	.008518	.004055		.82	.005798	.005929	−.004516
	.86	.005939	.008057	.003678		.86	.005256	.005641	−.004125
	.90	.005332	.007609	.003335		.90	.004775	.005358	−.003771
	.94	.004790	.007179	.003025		.94	.004343	.005087	−.003451
	.98	.004306	.006766	.002742		.98	.003955	.004830	−.003162
	.102	.003876	.006371	.002486		1.02	.003609	.004580	−.002897
	1.04	.003678	.006180	.002368		1.04	.003450	.004459	−.002775
	1.10	.003150	.005640	.002046		1.10	.003020	.004113	−.002440
150	0.20	0.032520	0.08140	0.026075	330	0.20	0.029442	0.004526	−0.021421
	.40	.017111	.017584	.030359		.40	.012419	.011111	−.024670
	.50	.010969	.019039	.027460		.50	.006925	.011697	−.021266
	.60	.006190	.019034	.023851		.60	.003600	.011243	−.017605
	.70	.002417	.018049	.020077		.70	.001619	.010413	−.014454
	.74	.001172	.017440	.018558		.74	.001053	.010037	−.013340
	.78	.000085	.016742	.017068		.78	.000581	.009659	−.012315
	.82	−.000841	.015970	.015615		.82	.000183	.009283	−.011371
	.86	−.001614	.015145	.014215		.86	−.000151	.008911	−.010500
	.90	−.002241	.014289	.012886		.90	−.000432	.008546	−.009698
	.94	−.002735	.013421	.011639		.94	−.000674	.008185	−.008954
	.98	−.003109	.012558	.010481		.98	−.000883	.007821	−.008259
	1.02	−.003378	.011712	.009416		1.02	−.001055	.007473	−.007623
	1.04	−.003477	.011300	.008919		1.04	−.001135	.007297	−.007320
	1.10	−.003661	.010115	.007563		1.10	−.001323	.006790	−.006482

Table 3. Continued

(d) $r_m/R = 0.8125$; $\alpha = -4.0°$

ψ, deg	r/r_m	u/V_∞	v/V_∞	w/V_∞	ψ, deg	r/r_m	u/V_∞	v/V_∞	w/V_∞
0	0.20	0.029151	−0.000142	−0.024042	180	0.20	0.031823	−0.000205	0.035843
	.40	.008591	−.000124	−.032048		.40	.012188	−.000220	.048647
	.50	.002117	−.000093	−.028608		.50	.004249	−.000188	.047563
	.60	−.001182	−.000057	−.024462		.60	−.002136	−.000142	.044753
	.70	−.002837	−.000043	−.021071		.70	−.007763	−.000108	.040352
	.74	−.003249	−.000035	−.019885		.74	−.009670	−.000098	.038058
	.78	−.003586	−.000028	−.018800		.78	−.011302	−.000088	.035502
	.82	−.003876	−.000022	−.017803		.82	−.012618	−.000080	.032793
	.86	−.004132	−.000017	−.016874		.86	−.013597	−.000072	.029985
	.90	−.004361	−.000013	−.015995		.90	−.014242	−.000065	.027159
	.94	−.004565	−.000010	−.015155		.94	−.014589	−.000058	.024395
	.98	−.004739	−.000008	−.014341		.98	−.014629	−.000053	.021753
	1.02	−.004871	−.000002	−.013576		1.02	−.014437	−.000047	.019284
	1.04	−.004938	−.000001	−.013192		1.04	−.014269	−.000045	.018125
	1.10	−.005111	.000004	−.012121		1.10	−.013551	−.000038	.014972
30	0.20	0.029986	−0.003811	−0.019014	210	0.20	0.032068	−0.009442	0.028291
	.40	.013055	−.010131	−.023277		.40	.016576	−.018904	.031340
	.50	.007540	−.010748	−.020301		.50	.010467	−.020202	.028077
	.60	.004169	−.010389	−.016978		.60	.005714	−.019995	.024199
	.70	.002111	−.009699	−.014079		.70	.001985	−.018808	.020227
	.74	.001515	−.009377	−.013046		.74	.000763	−.018121	.018646
	.78	.001012	−.009051	−.012089		.78	−.000299	−.017349	.017103
	.82	.000585	−.008725	−.011202		.82	−.001198	−.016508	.015608
	.86	.000225	−.008403	−.010384		.86	−.001943	−.015620	.014175
	.90	−.000086	−.008081	−.009623		.90	−.002543	−.014707	.012821
	.94	−.000352	−.007763	−.008915		.94	−.003010	−.013787	.011555
	.98	−.000586	−.007441	−.008247		.98	−.003358	−.012878	.010384
	1.02	−.000783	−.007130	−.007635		1.02	−.003602	−.011992	.009310
	1.04	−.000874	−.006973	−.007341		1.04	−.003690	−.011562	.008810
	1.10	−.001094	−.006513	−.006524		1.10	−.003841	−.010330	.007450

Table 3. Continued

(d) Continued

ψ, deg	r/r_m	u/V_∞	v/V_∞	w/V_∞	ψ, deg	r/r_m	u/V_∞	v/V_∞	w/V_∞
60	0.20	0.031231	−0.001795	−0.008619	240	0.20	0.032137	−0.009422	0.014465
	.40	.018469	−.006334	−.010282		.40	.020193	−.013456	.011066
	.50	.013867	−.006828	−.008838		.50	.015512	−.012925	.008733
	.60	.010517	−.006653	−.007278		.60	.011850	−.011789	.006810
	.70	.008054	−.006177	−.005902		.70	.009027	−.010472	.005298
	.74	.007262	−.005949	−.005418		.74	.008093	−.009935	.004788
	.78	.006565	−.005714	−.004971		.78	.007258	−.009403	.004326
	.82	.005942	−.005473	−.004561		.82	.006509	−.008883	.003908
	.86	.005389	−.005233	−.004185		.86	.005839	−.008379	.003531
	.90	.004897	−.004993	−.003840		.90	.005241	−.007893	.003188
	.94	.004456	−.004760	−.003526		.94	.004707	−.007430	.002881
	.98	.004058	−.004536	−.003241		.98	.004231	−.006987	.002603
	1.02	.003705	−.004315	−.002980		1.02	.003807	−.006566	.002352
	1.04	.003542	−.004208	−.002857		1.04	.003613	−.006365	.002236
	1.10	.003100	−.003899	−.002523		1.10	.003093	−.005794	.001923
90	0.20	0.031868	0.003909	0.002447	270	0.20	0.031817	−0.004016	0.002242
	.40	.020525	.003031	−.000257		.40	.020491	−.002981	−.000409
	.50	.016200	.002357	−.000628		.50	.016166	−.002297	−.000740
	.60	.012833	.001804	−.000736		.60	.012805	−.001742	−.000815
	.70	.010243	.001392	−.000716		.70	.010220	−.001334	−.000771
	.74	.009384	.001259	−.000691		.74	.009363	−.001204	−.000739
	.78	.008609	.001142	−.000662		.78	.008589	−.001091	−.000704
	.82	.007909	.001039	−.000630		.82	.007891	−.000991	−.000667
	.86	.007281	.000947	−.000598		.86	.007265	−.000902	−.000630
	.90	.006708	.000865	−.000565		.90	.006693	−.000823	−.000593
	.94	.006189	.000792	−.000533		.94	.006175	−.000753	−.000557
	.98	.005721	.000725	−.000502		.98	.005708	−.000689	−.000524
	1.02	.005295	.000666	−.000473		1.02	.005283	−.000633	−.000492
	1.04	.005096	.000639	−.000458		1.04	.005084	−.000607	−.000476
	1.10	.004553	.000565	−.000418		1.10	.004542	−.000537	−.000433

Table 3. Concluded

(d) Concluded

ψ, deg	r/r_m	u/V_∞	v/V_∞	w/V_∞	ψ, deg	r/r_m	u/V_∞	v/V_∞	w/V_∞
120	0.20	0.032207	0.009280	0.014704	300	0.20	0.031214	0.001645	−0.008799
	.40	.020237	.013492	.011294		.40	.018438	.006364	−.010448
	.50	.015528	.013005	.008914		.50	.013824	.006891	−.008961
	.60	.011850	.011873	.006940		.60	.010468	.006710	−.007364
	.70	.009018	.010548	.005390		.70	.008006	.006225	−.005954
	.74	.008082	.010007	.004868		.74	.007216	.005993	−.005461
	.78	.007246	.009471	.004397		.78	.006521	.005753	−.005006
	.82	.006497	.008946	.003970		.82	.005901	.005507	−.004590
	.86	.005827	.008438	.003585		.86	.005350	.005262	−.004208
	.90	.005228	.007947	.003236		.90	.004861	.005018	−.003859
	.94	.004694	.007480	.002923		.94	.004422	.004782	−.003542
	.98	.004218	.007034	.002640		.98	.004027	.004555	−.003255
	1.02	.003795	.006610	.002385		1.02	.003676	.004332	−.002991
	1.04	.003601	.006406	.002267		1.04	.003514	.004224	−.002867
	1.10	.003082	.005831	.001949		1.10	.003075	.003912	−.002531
150	0.20	0.032132	0.009157	0.028510	330	0.20	0.029987	0.003583	−0.019155
	.40	.016544	.018805	.031731		.40	.013001	.010046	−.023486
	.50	.010385	.020161	.028394		.50	.007451	.010726	−.020467
	.60	.005624	.019988	.024429		.60	.004064	.010394	−.017086
	.70	.001901	.018814	.020392		.70	.002023	.009697	−.014140
	.74	.000684	.018129	.018791		.74	.001433	.009375	−.013090
	.78	−.000374	.017359	.017232		.78	.000938	.009049	−.012120
	.82	−.001268	.016520	.015722		.82	.000518	.008722	−.011223
	.86	−.002009	.015633	.014276		.86	.000163	.008398	−.010393
	.90	−.002605	.014720	.012910		.90	−.000137	.008077	−.009625
	.94	−.003068	.013801	.011634		.94	−.000399	.007758	−.008911
	.98	−.003413	.012891	.010454		.98	−.000627	.007434	−.008239
	1.02	−.003653	.012005	.009372		1.02	−.000818	.007123	−.007623
	1.04	−.003740	.011575	.008868		1.04	−.000906	.006965	−.007328
	1.10	−.003887	.010341	.007498		1.10	−.001120	.006504	−.006510

Table 4. Induced Velocity Perturbations of Fuselage and Hub Computed at Inflow Measurement Plane

$[r_m/R = 0.8470; \alpha = -3.0°]$

ψ, deg	r/r_m	u/V_∞	v/V_∞	w/V_∞	ψ, deg	r/r_m	u/V_∞	v/V_∞	w/V_∞
0	0.20	−0.003858	0.000231	−0.125306	180	0.20	−0.010468	0.000233	0.147124
	.40	−.013455	−.000116	−.047204		.40	−.012023	−.000239	.060708
	.50	−.011484	−.000101	−.035480		.50	−.009735	−.000174	.051497
	.60	−.009927	−.000066	−.027879		.60	−.011014	−.000131	.045533
	.70	−.008813	−.000051	−.022889		.70	−.013723	−.000099	.039392
	.74	−.008453	−.000043	−.021292		.74	−.014732	−.000089	.036587
	.78	−.008160	−.000035	−.019879		.78	−.015568	−.000080	.033674
	.82	−.007924	−.000029	−.018607		.82	−.016158	−.000072	.030680
	.86	−.007734	−.000024	−.017442		.86	−.016478	−.000064	.027684
	.90	−.007579	−.000020	−.016360		.90	−.016545	−.000058	.024766
	.94	−.007444	−.000016	−.015339		.94	−.016338	−.000052	.021987
	.98	−.007307	−.000010	−.014391		.98	−.015924	−.000046	.019404
	1.02	−.007199	−.000007	−.013485		1.02	−.015349	−.000041	.017044
	1.04	−.007150	−.000005	−.013058		1.04	−.015016	−.000039	.015953
	1.10	−.006984	−.000002	−.011810		1.10	−.013896	−.000033	.013035
30	0.20	0.019383	−0.043685	−0.107474	210	0.20	0.016630	−0.057727	0.122390
	.40	−.000418	−.025524	−.035721		.40	.002066	−.034533	.041106
	.50	−.000979	−.019871	−.025632		.50	.001889	−.028347	.031255
	.60	−.001417	−.016114	−.019323		.60	.000206	−.024438	.024996
	.70	−.001729	−.013443	−.015030		.70	−.001744	−.021180	.019984
	.74	−.001826	−.012568	−.013663		.74	−.002444	−.019931	.018179
	.78	−.001913	−.011780	−.012449		.78	−.003054	−.018701	.016475
	.82	−.001987	−.011064	−.011365		.82	−.003564	−.017487	.014870
	.86	−.002050	−.010410	−.010393		.86	−.003968	−.016298	.013373
	.90	−.002103	−.009804	−.009510		.90	−.004268	−.015144	.011989
	.94	−.002153	−.009232	−.008699		.94	−.004471	−.014035	.010719
	.98	−.002189	−.008705	−.007971		.98	−.004589	−.012977	.009563
	1.02	−.002218	−.008205	−.007299		1.02	−.004633	−.011978	.008519
	1.04	−.002228	−.007969	−.006988		1.04	−.004632	−.011502	.008038
	1.10	−.002240	−.007293	−.006129		1.10	−.004553	−.010170	.006744

Table 4. Continued

ψ, deg	r/r_m	u/V_∞	v/V_∞	w/V_∞	ψ, deg	r/r_m	u/V_∞	v/V_∞	w/V_∞
60	0.20	0.067178	−0.041777	−0.062326	240	0.20	0.068858	−0.057459	0.065002
	.40	.021649	−.021614	−.017492		.40	.023747	−.028066	.015930
	.50	.014958	−.015785	−.011817		.50	.016932	−.020498	.010416
	.60	.010835	−.012182	−.008509		.60	.012386	−.016025	.007439
	.70	.008057	−.009743	−.006358		.70	.009168	−.012948	.005517
	.74	.007203	−.008972	−.005695		.74	.008149	−.011941	.004919
	.78	.006456	−.008287	−.005118		.78	.007251	−.011040	.004397
	.82	.005803	−.007676	−.004610		.82	.006457	−.010221	.003937
	.86	.005230	−.007123	−.004162		.86	.005756	−.009475	.003528
	.90	.004725	−.006621	−.003766		.90	.005138	−.008793	.003166
	.94	.004275	−.006170	−.003415		.94	.004592	−.008168	.002844
	.98	.003879	−.005754	−.003102		.98	.004109	−.007592	.002557
	1.02	.003527	−.005373	−.002822		1.02	.003683	−.007061	.002300
	1.04	.003364	−.005194	−.002694		1.04	.003489	−.006812	.002183
	1.10	.002928	−.004701	−.002347		1.10	.002973	−.006123	.001868
90	0.20	0.093008	0.006021	−0.001777	270	0.20	0.093084	−0.007733	−0.000741
	.40	.032285	.002224	−.001405		.40	.032297	−.002339	−.001601
	.50	.022191	.001502	−.001174		.50	.022173	−.001494	−.001326
	.60	.016140	.001124	−.000944		.60	.016124	−.001083	−.001045
	.70	.012175	.000872	−.000761		.70	.012162	−.000826	−.000829
	.74	.010961	.000792	−.000698		.74	.010948	−.000745	−.000758
	.78	.009903	.000724	−.000640		.78	.009891	−.000678	−.000691
	.82	.008980	.000663	−.000588		.82	.008969	−.000620	−.000632
	.86	.008163	.000610	−.000540		.86	.008153	−.000569	−.000578
	.90	.007441	.000563	−.000497		.90	.007432	−.000523	−.000530
	.94	.006803	.000519	−.000458		.94	.006794	−.000482	−.000487
	.98	.006234	.000480	−.000423		.98	.006225	−.000445	−.000448
	1.02	.005724	.000444	−.000391		1.02	.005717	−.000412	−.000413
	1.04	.005489	.000428	−.000376		1.04	.005482	−.000397	−.000397
	1.10	.004856	.000384	−.000335		1.10	.004849	−.000356	−.000353

Table 4. Concluded

ψ, deg	r/r_m	u/V_∞	v/V_∞	w/V_∞	ψ, deg	r/r_m	u/V_∞	v/V_∞	w/V_∞
120	0.20	0.069952	0.056236	0.064087	300	0.20	0.068251	0.040711	−0.061515
	.40	.023794	.027974	.016199		.40	.021740	.021562	−.017706
	.50	.016370	.020540	.010623		.50	.014959	.015821	−.011986
	.60	.012391	.016092	.007580		.60	.010806	.012234	−.008625
	.70	.009159	.013012	.005614		.70	.008022	.009792	−.006430
	.74	.008138	.012003	.005002		.74	.007168	.009018	−.005755
	.78	.007238	.011098	.004469		.78	.006421	.008329	−.005167
	.82	.006443	.010276	.003998		.82	.005769	.007713	−.004652
	.86	.005742	.009527	.003583		.86	.005197	.007156	−.004197
	.90	.005124	.008841	.003214		.90	.004694	.006651	−.003796
	.94	.004577	.008212	.002886		.94	.004247	.006197	−.003441
	.98	.004095	.007633	.002593		.98	.003852	.005778	−.003124
	1.02	.003670	.007100	.002333		1.02	.003501	.005395	−.002841
	1.04	.003476	.006849	.002213		1.04	.003340	.005215	−.002711
	1.10	.002961	.006156	.001893		1.10	.002906	.004719	−.002361
150	0.20	0.017812	0.057633	0.121920	330	0.20	0.020389	0.043674	−0.107096
	.40	.002091	.034398	.041512		.40	−.000371	.025474	−.035990
	.50	.001824	.028312	.031578		.50	−.001049	.019842	−.025836
	.60	.000123	.024433	.025219		.60	−.001514	.016123	−.019475
	.70	−.001823	.021184	.020139		.70	−.001817	.013443	−.015113
	.74	−.002518	.019939	.018315		.74	−.001908	.012568	−.013727
	.78	−.003124	.018710	.016595		.78	−.001988	.011778	−.012496
	.82	−.003630	.017497	.014975		.82	−.002054	.011063	−.011400
	.86	−.004030	.016310	.013465		.86	−.002109	.010408	−.010415
	.90	−.004326	.015156	.012070		.90	−.002156	.009803	−.009526
	.94	−.004526	.014046	.010790		.94	−.002201	.009229	−.008709
	.98	−.004640	.012989	.009626		.98	−.002230	.008701	−.007975
	1.02	−.004681	.011989	.008574		1.02	−.002255	.008200	−.007301
	1.04	−.004679	.011513	.008089		1.04	−.002261	.007963	−.006989
	1.10	−.004595	.010179	.006786		1.10	−.002267	.007286	−.006127

Table 5. Induced Velocity Perturbations of Ellipsoid Fuselage Computed at Inflow Measurement Plane

$[r_m/R = 0.8470; \alpha = -3.0°]$

ψ, deg	r/r_m	u/V_∞	v/V_∞	w/V_∞	ψ, deg	r/r_m	u/V_∞	v/V_∞	w/V_∞
0	0.20	0.011207	0.000000	0.004913	180	0.20	0.007893	0.000000	0.015063
	.40	.011188	.000000	−.000409		.40	.004059	.000001	.018593
	.50	.010824	.000001	−.002970		.50	.001541	.000002	.019375
	.60	.010220	.000001	−.005421		.60	−.001206	.000001	.019159
	.70	.009379	.000001	−.007713		.70	−.003846	−.000001	.017770
	.74	.008973	.000001	−.008582		.74	−.004768	−.000001	.016887
	.78	.008530	.000001	−.009411		.78	−.005563	−.000001	.015839
	.82	.008044	.000002	−.010200		.82	−.006206	−.000001	.014671
	.86	.007518	.000002	−.010940		.86	−.006681	−.000001	.013429
	.90	.006949	.000002	−.011626		.90	−.006986	−.000001	.012160
	.94	.006341	.000002	−.012256		.94	−.007132	−.000001	.010899
	.98	.005693	.000002	−.012820		.98	−.007132	−.000001	.009693
	1.02	.005007	.000002	−.013314		1.02	−.007020	−.000001	.008571
	1.04	.004652	.000002	−.013533		1.04	−.006925	−.000001	.008046
	1.10	.003541	.000002	−.014062		1.10	−.006542	.000000	.006627
30	0.20	0.010864	0.001302	0.005293	210	0.20	0.008049	−0.003063	0.013638
	.40	.010314	.000651	.000642		.40	.004682	−.006331	.014164
	.50	.009688	−.000153	−.001201		.50	.002793	−.007432	.013306
	.60	.008889	−.001093	−.002642		.60	.000996	−.007959	.011868
	.70	.007954	−.002050	−.003684		.70	−.000514	−.007894	.010080
	.74	.007553	−.002415	−.003995		.74	−.001006	−.007725	.009327
	.78	.007139	−.002762	−.004250		.78	−.001428	−.007486	.008572
	.82	.006718	−.003086	−.004450		.82	−.001777	−.007195	.007832
	.86	.006290	−.003384	−.004600		.86	−.002054	−.006864	.007121
	.90	.005859	−.003655	−.004704		.90	−.002264	−.006508	.006447
	.94	.005427	−.003895	−.004765		.94	−.002414	−.006138	.005818
	.98	.004997	−.004103	−.004787		.98	−.002510	−.005760	.005234
	1.02	.004570	−.004279	−.004774		1.02	−.002562	−.005390	.004702
	1.04	.004359	−.004355	−.004755		1.04	−.002572	−.005207	.004453
	1.10	.003741	−.004529	−.004653		1.10	−.002553	−.004684	.003783

Table 5. Continued

ψ, deg	r/r_m	u/V_∞	v/V_∞	w/V_∞	ψ, deg	r/r_m	u/V_∞	v/V_∞	w/V_∞
60	0.20	0.010068	0.002625	0.006380	240	0.20	0.008508	−0.004221	0.010754
	.40	.008680	.002372	.002585		.40	.005892	−.006513	.008298
	.50	.007800	.001743	.001321		.50	.004640	−.006695	.006812
	.60	.006907	.001070	.000458		.60	.003557	−.006445	.005451
	.70	.006049	.000465	−.000092		.70	.002675	−.005941	.004295
	.74	.005722	.000252	−.000246		.74	.002376	−.005701	.003893
	.78	.005406	.000058	−.000370		.78	.002107	−.005449	.003525
	.82	.005101	−.000118	−.000468		.82	.001867	−.005192	.003190
	.86	.0048^	−.000275	−.000543		.86	.001653	−.004934	.002886
	.90	.004528	−.000412	−.000600		.90	.001463	−.004680	.002612
	.94	.004260	−.000533	−.000641		.94	.001295	−.004430	.002363
	.98	.004005	−.000637	−.000668		.98	.001147	−.004188	.002139
	1.02	.003762	−.000726	−.000685		1.02	.001018	−.003954	.001937
	1.04	.003645	−.000765	−.000690		1.04	.000959	−.003841	.001844
	1.10	.003313	−.000863	−.000694		1.10	.000804	−.003518	.001592
90	0.20	0.009211	0.003773	0.008177	270	0.20	0.009210	−0.003773	0.008176
	.40	.007192	.004541	.004823		.40	.007191	−.004540	.004822
	.50	.006189	.004216	.003532		.50	.006188	−.004215	.003531
	.60	.005282	.003728	.002560		.60	.005281	−.003727	.002559
	.70	.004496	.003207	.001852		.70	.004496	−.003206	.001852
	.74	.004216	.003004	.001628		.74	.004215	−.003004	.001627
	.78	.003952	.002809	.001431		.78	.003951	−.002809	.001431
	.82	.003705	.002622	.001259		.82	.003705	−.002622	.001259
	.86	.003475	.002445	.001109		.86	.003475	−.002445	.001108
	.90	.003262	.002278	.000977		.90	.003261	−.002278	.000977
	.94	.003063	.002122	.000862		.94	.003062	−.002122	.000862
	.98	.002877	.001975	.000761		.98	.002876	−.001974	.000760
	1.02	.002704	.001837	.000672		1.02	.002703	−.001837	.000672
	1.04	.002622	.001771	.000632		1.04	.002622	−.001771	.000631
	1.10	.002393	.001589	.000525		1.10	.002393	−.001588	.000525

Table 5. Concluded

ψ, deg	r/r_m	u/V_∞	v/V_∞	w/V_∞	ψ, deg	r/r_m	u/V_∞	v/V_∞	w/V_∞
120	0.20	0.008508	0.004222	0.010754	300	0.20	0.010067	−0.002624	0.006380
	.40	.005892	.006515	.008300		.40	.008679	−.002372	.002585
	.50	.004641	.006696	.006813		.50	.007798	−.001743	.001321
	.60	.003557	.006445	.005452		.60	.006906	−.001070	.000458
	.70	.002675	.005942	.004296		.70	.006048	−.000465	−.000092
	.74	.002376	.005701	.003894		.74	.005721	−.000252	−.000246
	.78	.002107	.005450	.003526		.78	.005405	−.000058	−.000370
	.82	.001867	.005193	.003191		.82	.005101	.000118	−.000468
	.86	.001653	.004935	.002887		.86	.004808	.000275	−.000543
	.90	.001463	.004681	.002613		.90	.004527	.000412	−.000600
	.94	.001295	.004431	.002364		.94	.004259	.000533	−.000640
	.98	.001147	.004188	.002140		.98	.004004	.000637	−.000668
	1.02	.001018	.003955	.001937		1.02	.003761	.000726	−.000685
	1.04	.000959	.003841	.001844		1.04	.003645	.000765	−.000690
	1.10	.000804	.003518	.001592		1.10	.003313	.000863	−.000694
150	0.20	0.008049	0.003063	0.013638	330	0.20	0.010864	−0.001302	0.005293
	.40	.004682	.006331	.014165		.40	.010314	−.000651	.000642
	.50	.002792	.007433	.013308		.50	.009687	.000153	−.001201
	.60	.000997	.007959	.011871		.60	.008888	.001093	−.002641
	.70	−.000515	.007894	.010082		.70	.007953	.002050	−.003683
	.74	−.001007	.007725	.009329		.74	.007552	.002415	−.003994
	.78	−.001429	.007486	.008574		.78	.007138	.002762	−.004249
	.82	−.001778	.007195	.007834		.82	.006717	.003086	−.004449
	.86	−.002056	.006865	.007122		.86	.006289	.003384	−.004599
	.90	−.002265	.006508	.006449		.90	.005859	.003655	−.004703
	.94	−.002415	.006138	.005819		.94	.005427	.003895	−.004764
	.98	−.002511	.005761	.005235		.98	.004996	.004103	−.004786
	1.02	−.002562	.005390	.004703		1.02	.004570	.004278	−.004772
	1.04	−.002573	.005207	.004454		1.04	.004359	.004354	−.004754
	1.10	−.002553	.004684	.003784		1.10	.003741	.004529	−.004651
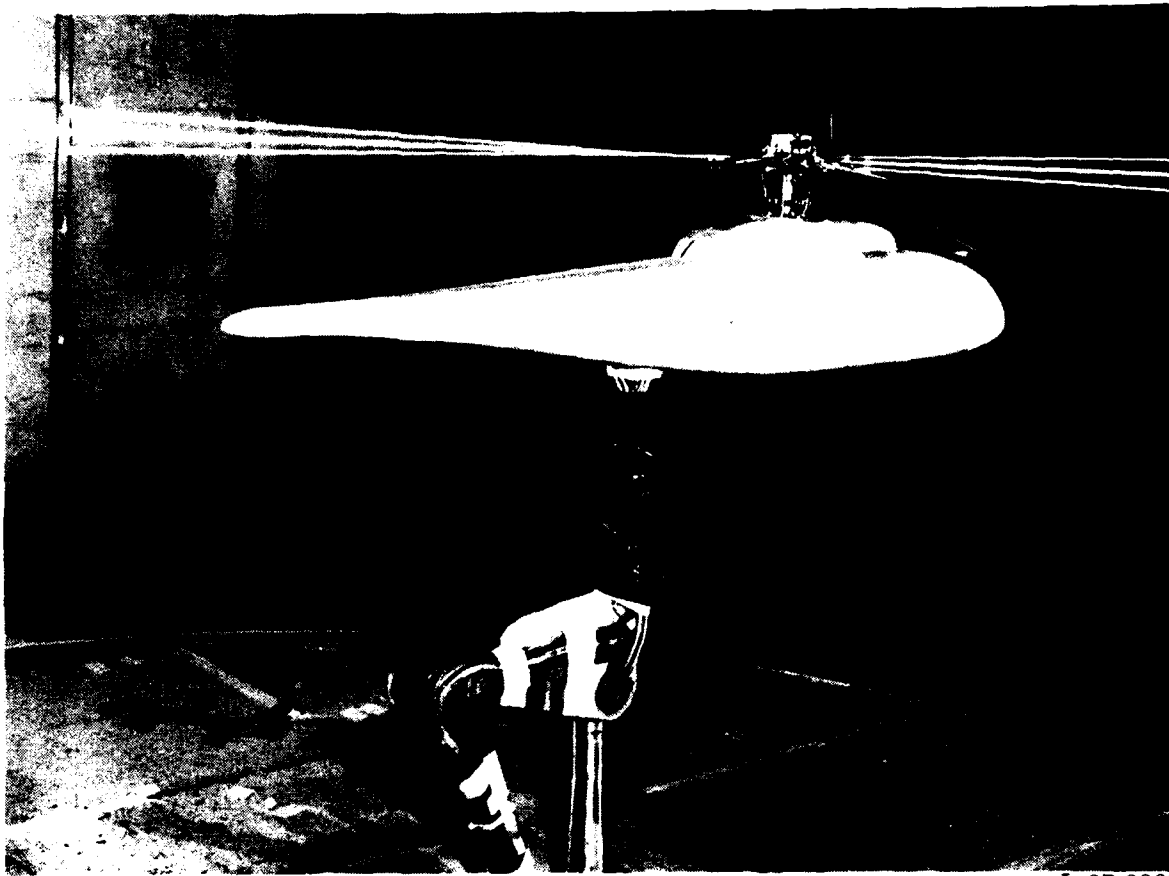
Figure 1. ROBIN fuselage in the Langley 14- by 22-Foot Subsonic Tunnel.
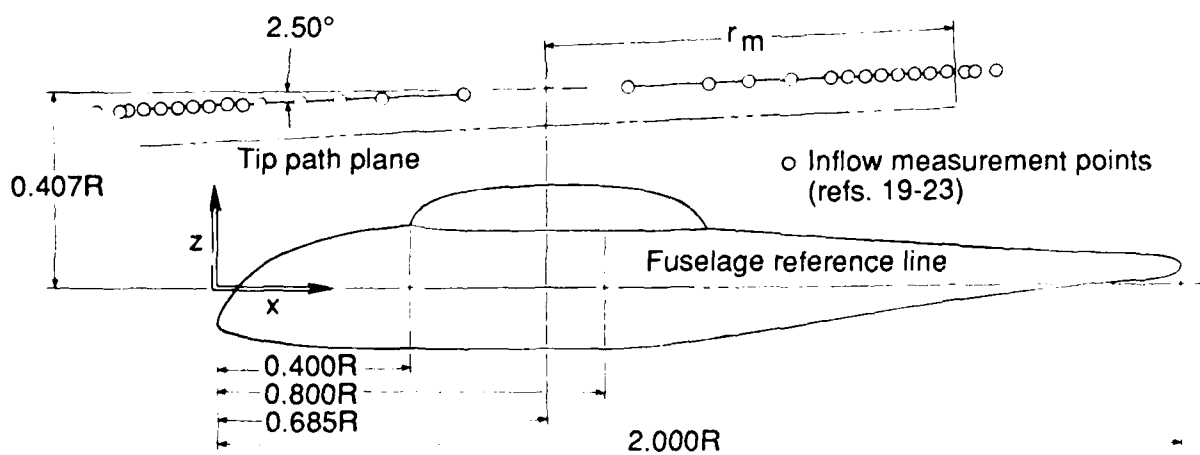
Figure 2. Fuselage coordinate system.
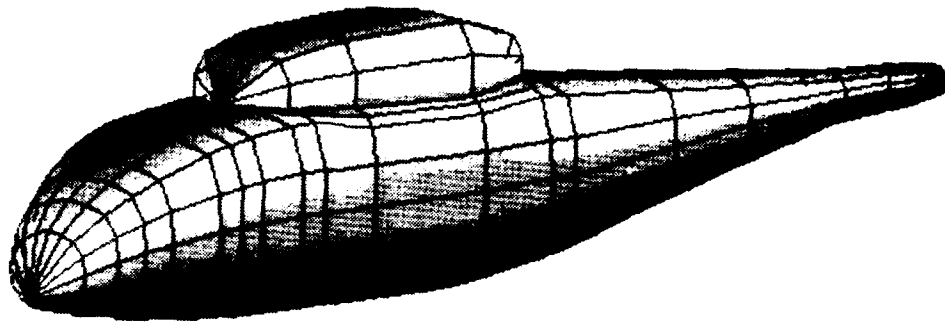
Figure 3. ROBIN fuselage with nacelle panel configuration.
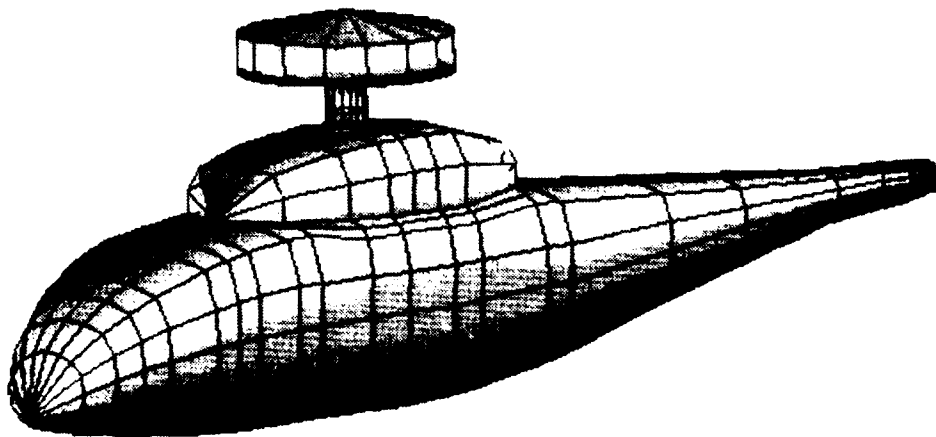
Figure 4. ROBIN fuselage with nacelle and hub panel configuration.
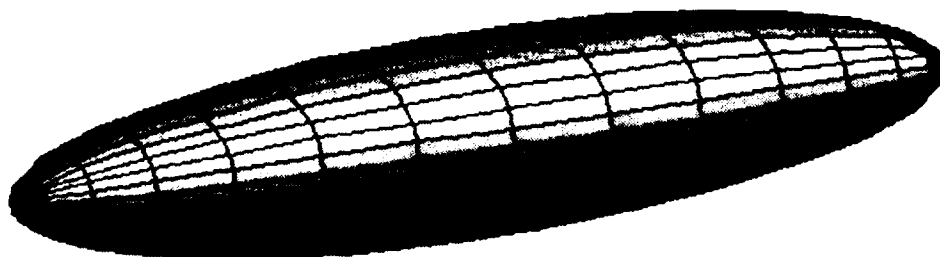
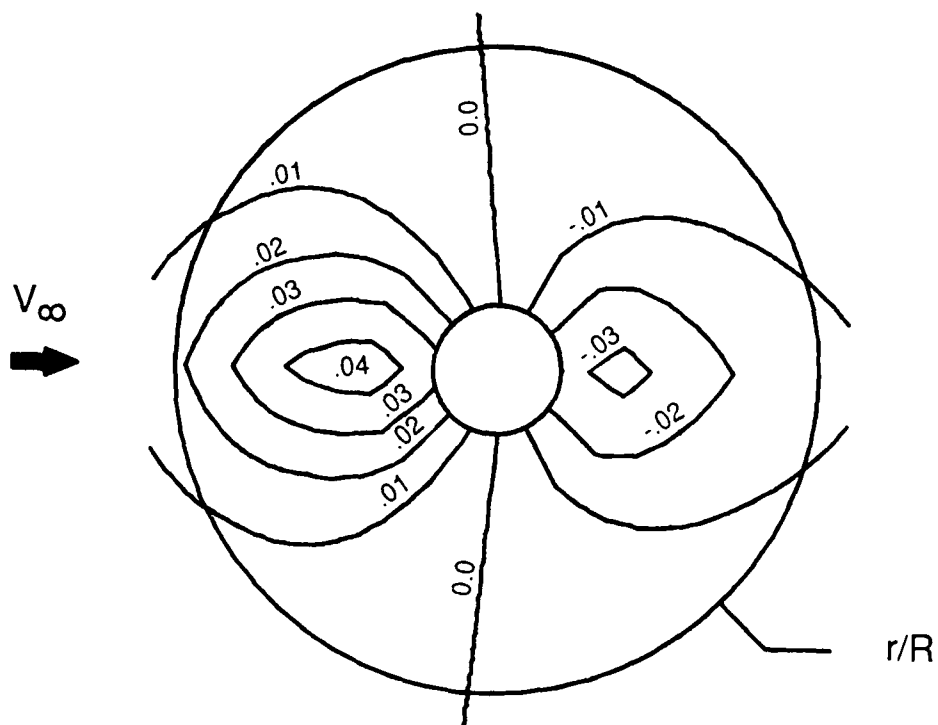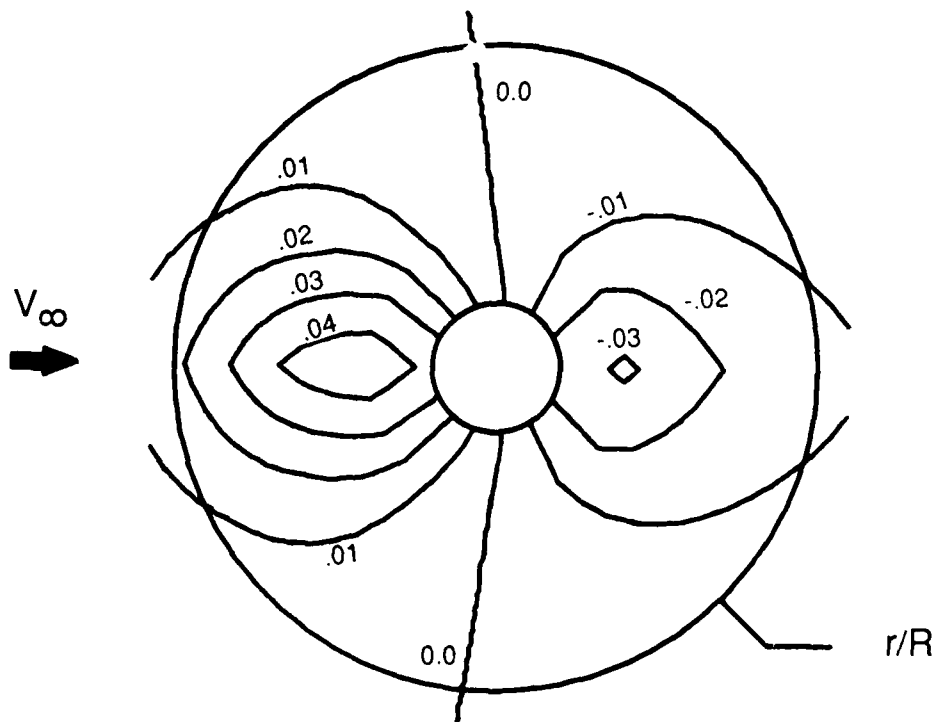Figure 5. Ellipsoid fuselage panel configuration.
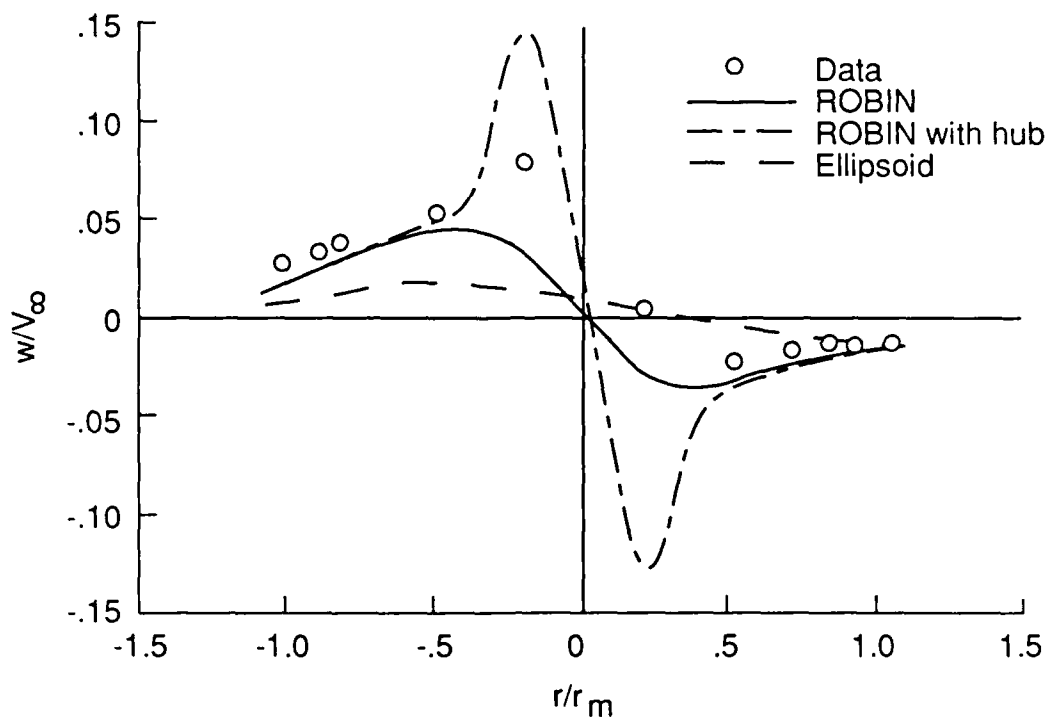
(a) Normal component.
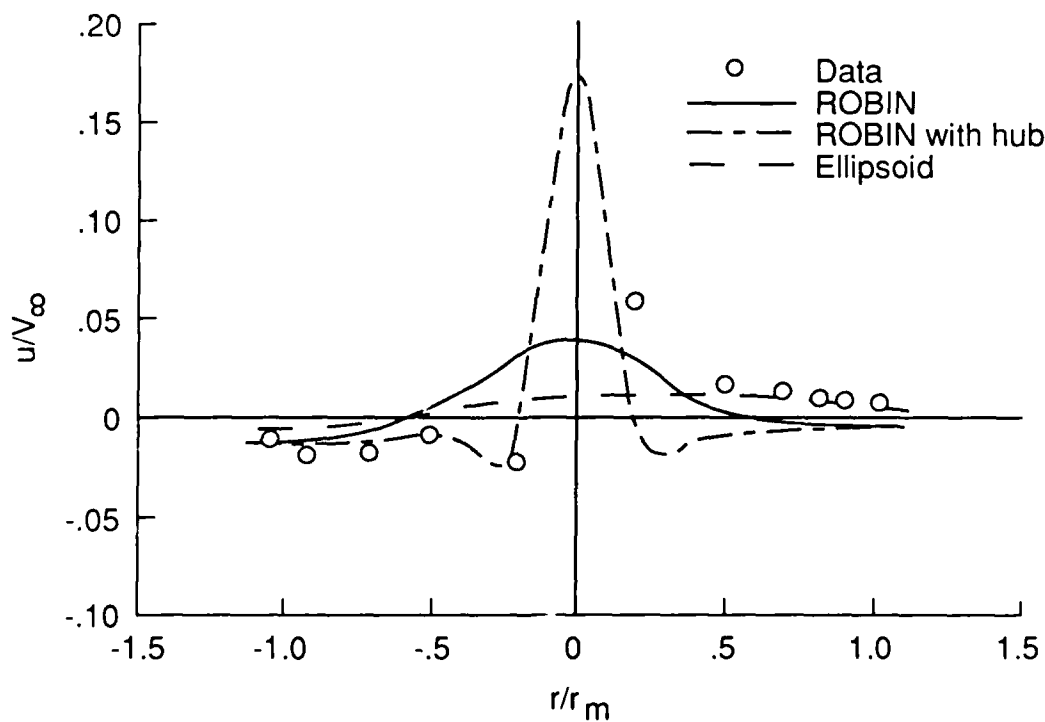
(b) Tangential component.

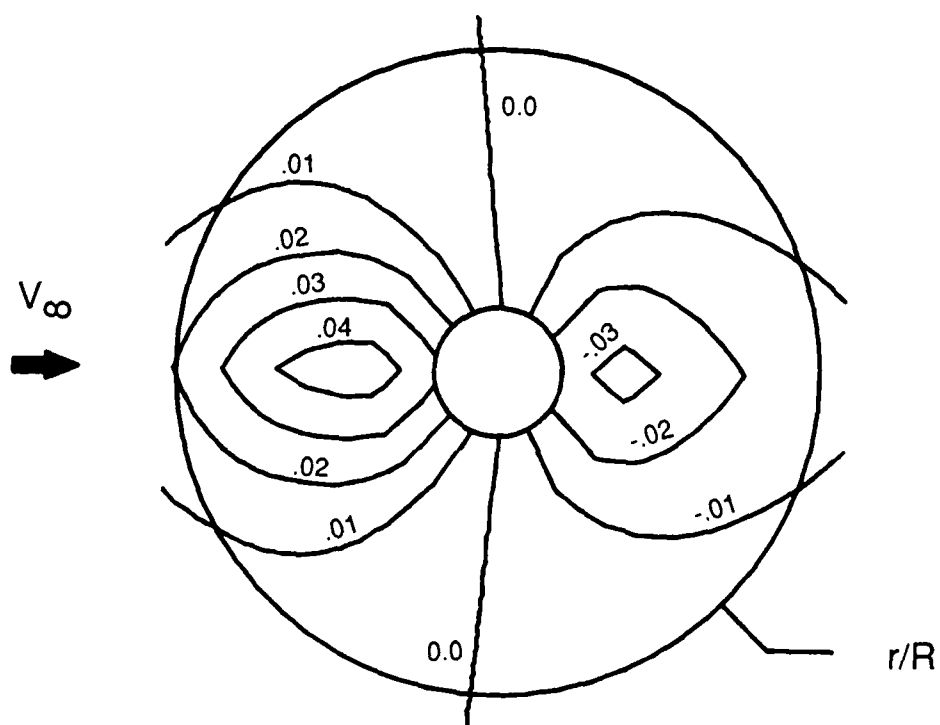Figure 6. Velocity perturbations over fuselage centerline.
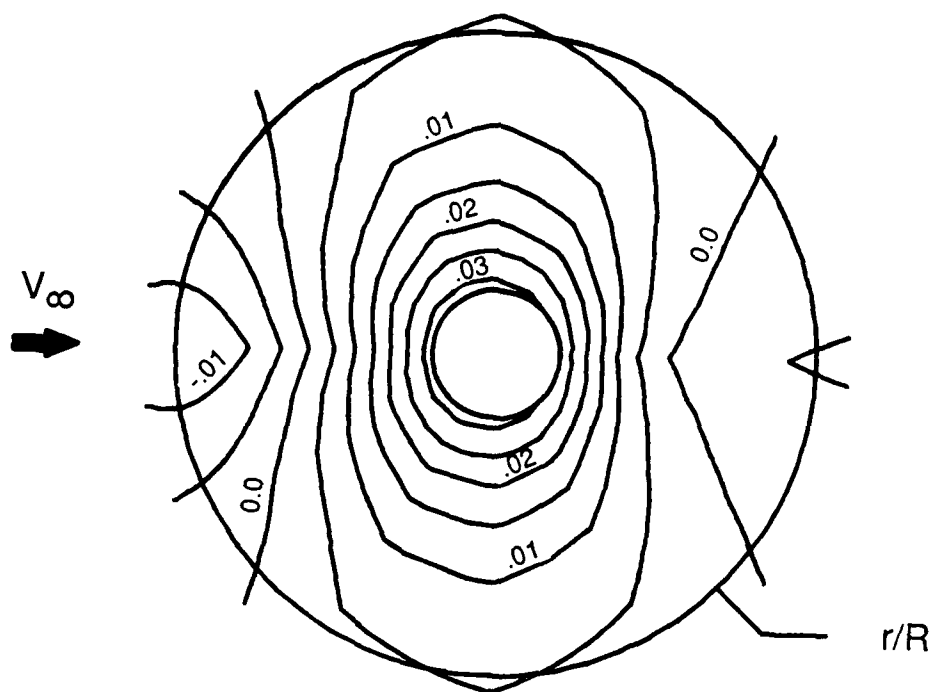
(a) $\alpha = -3.0°$; $r_m/R = 0.8470$.

(b) $\alpha = -4.0°$; $r_m/R = 0.8470$.

Figure 7. Normal velocity perturbations computed at inflow measurement plane.

53

(c) $\alpha = -3.0°$; $r_m/R = 0.8125$.

Figure 7. Concluded.

(a) *u*-component due to ROBIN fuselage-nacelle configuration.
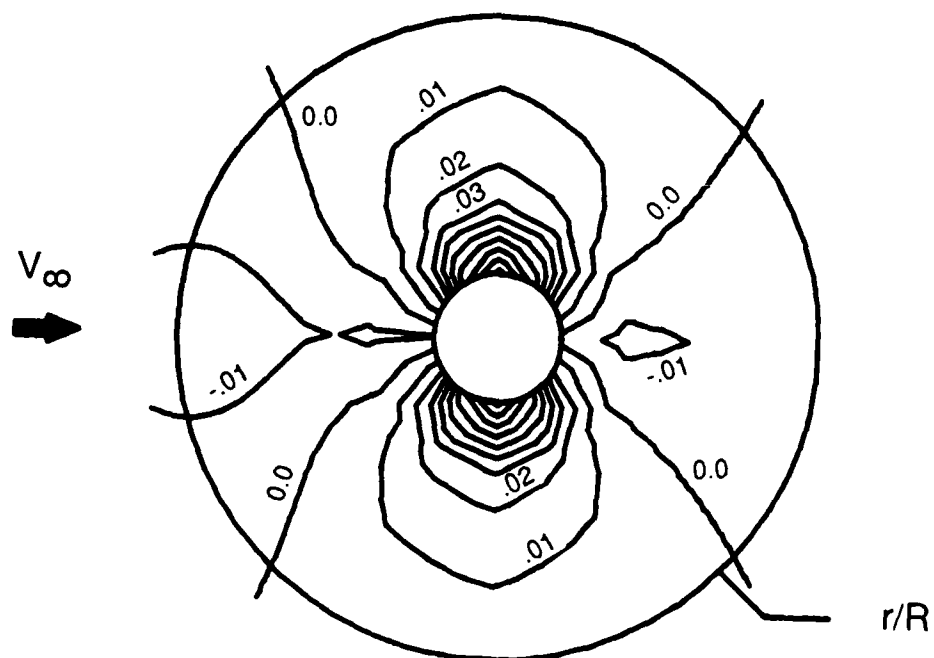
(b) *u*-component due to ROBIN and hub.

Figure 8. Downstream tangential perturbation velocities computed at inflow measurement plane for $\alpha = -3.0°$ and $r_m/R = 0.8470$.
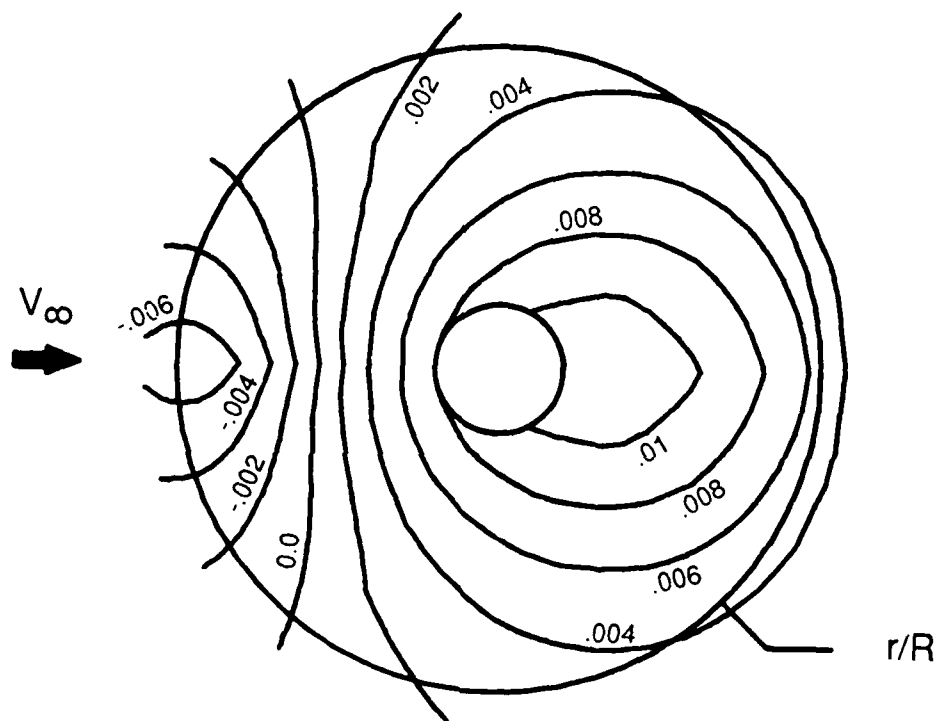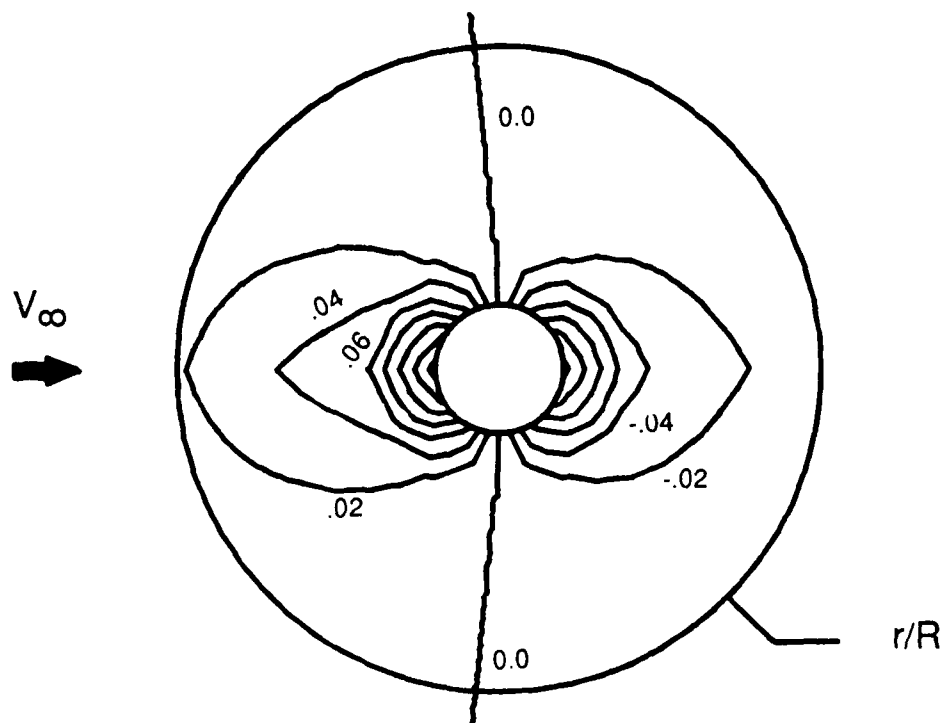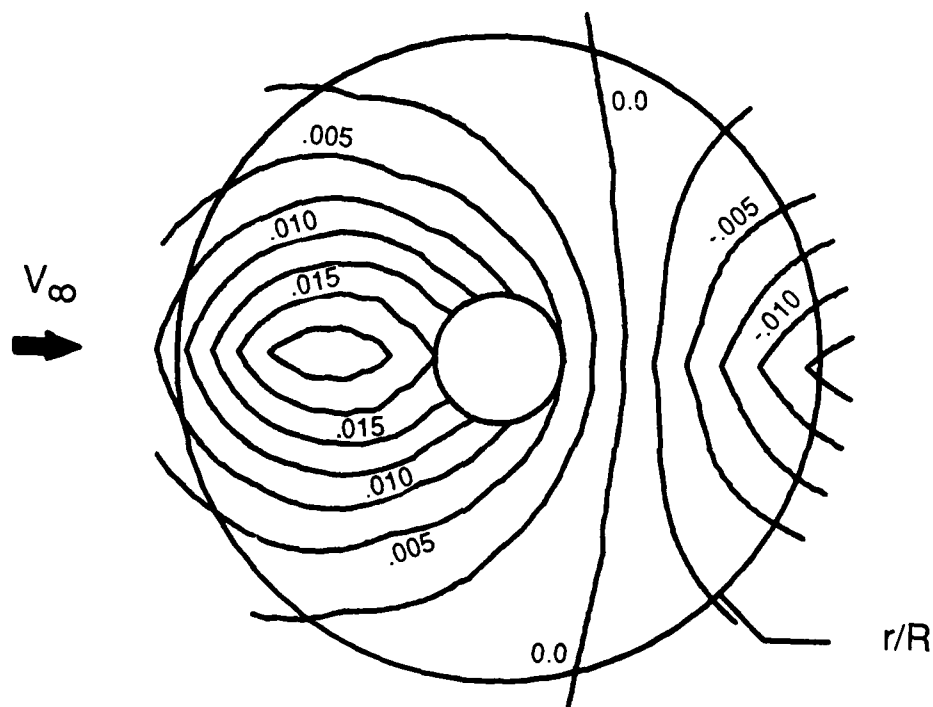
(c) u-component due to ellipsoid.

Figure 8. Concluded.
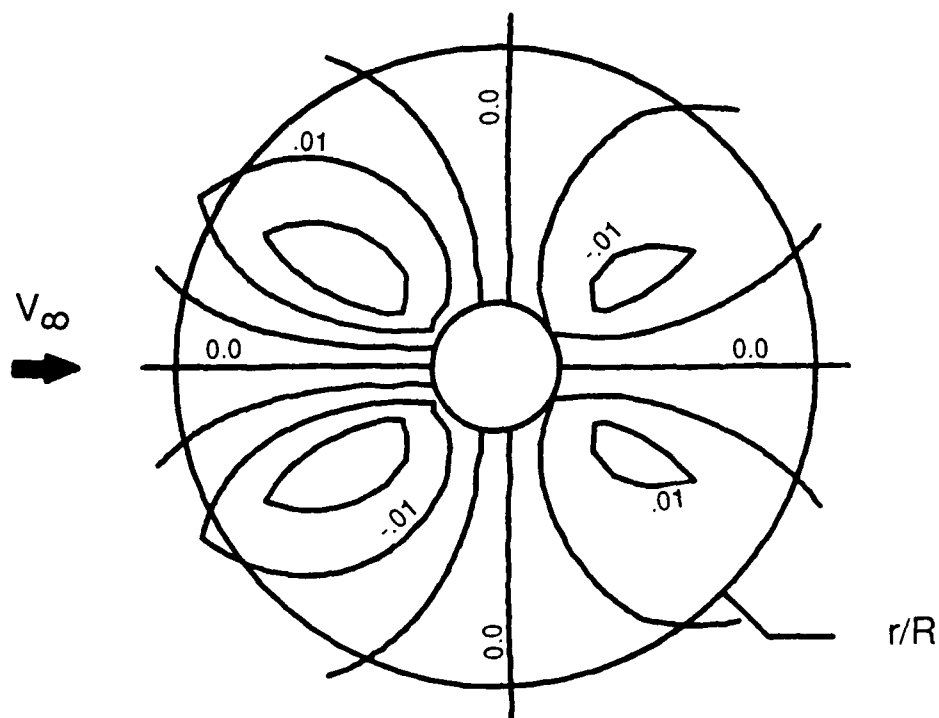
(a) v-component due to ROBIN fuselage-nacelle configuration.
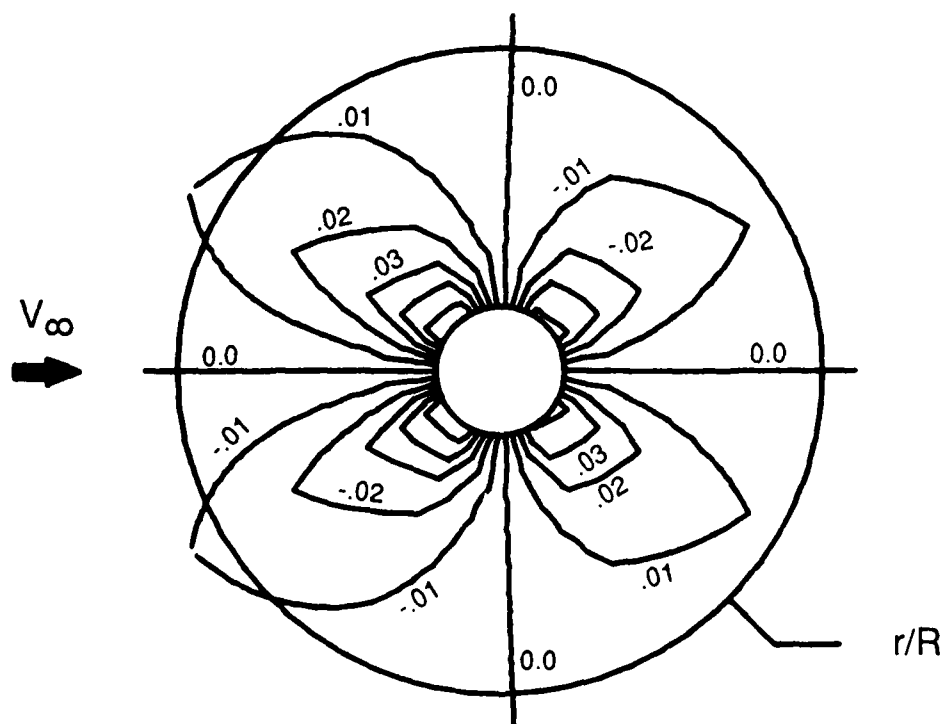
(b) v-component due to ROBIN and hub.

Figure 9. Lateral tangential perturbation velocities computed at inflow measurement plane for $\alpha = -3.0°$ and $r_m/R = 0.8470$.
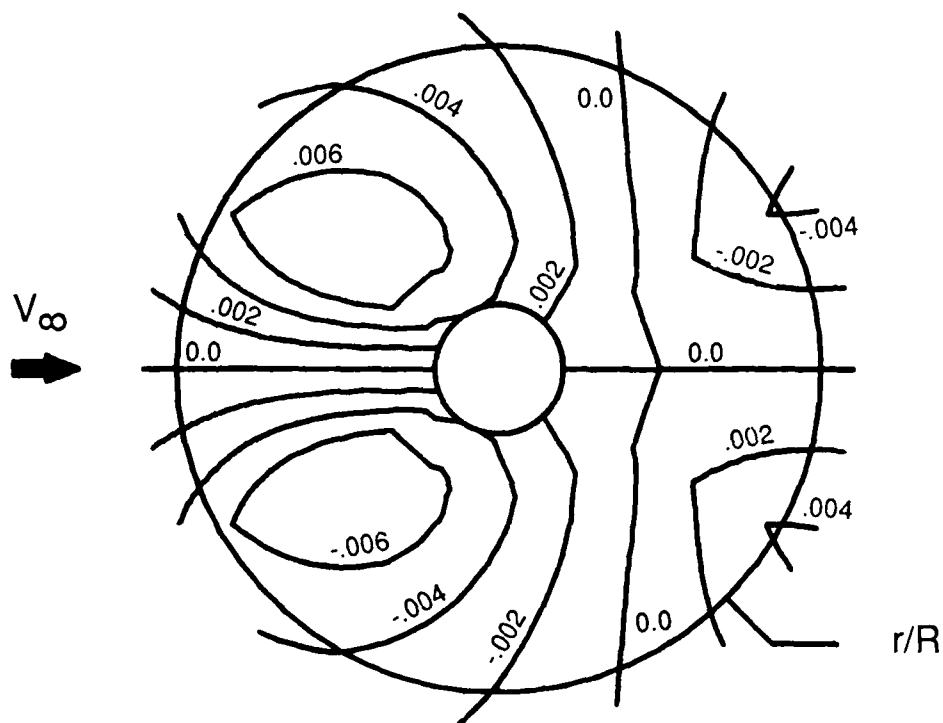
(c) v-component due to ellipsoid.

Figure 9. Concluded.
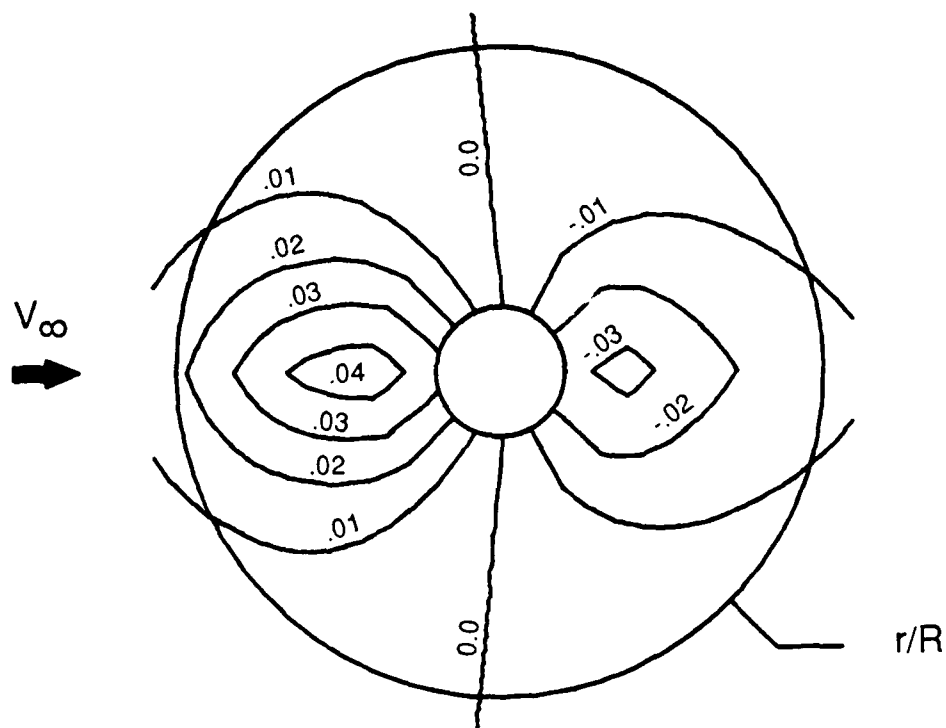
(a) w-component due to ROBIN fuselage-nacelle configuration. Map same as that of figure 7(a).

(b) w-component due to ROBIN and hub.

Figure 10. Normal perturbation velocities computed at inflow measurement plane for $\alpha = -3.0°$ and $r_m/R = 0.8470$.

(c) *w*-component due to ellipsoid.

Figure 10. Concluded.

NASA

National Aeronautics and
Space Administration

Report Documentation Page

1. Report No. NASA TM-4113 AVSCOM TR 89-B-001	2. Government Accession No.	3. Recipient's Catalog No.

4. Title and Subtitle		5. Report Date
Computing Induced Velocity Perturbations Due to a Helicopter Fuselage in a Free Stream		JUNE 1989
		6. Performing Organization Code

7. Author(s)	8. Performing Organization Report No.
John D. Berry and Susan L. Althoff	L-16533

9. Performing Organization Name and Address	10. Work Unit No.
Aerostructures Directorate USAARTA-AVSCOM	505-61-51-10
Langley Research Center Hampton, VA 23665-5225	11. Contract or Grant No.

12. Sponsoring Agency Name and Address	13. Type of Report and Period Covered
National Aeronautics and Space Administration Washington, DC 20546-0001 and	Technical Memorandum
	14. Army Project No.
U.S. Army Aviation Systems Command St. Louis, MO 63120-1798	1L162211A47A

15. Supplementary Notes

John D. Berry and Susan L. Althoff: Aerostructures Directorate, USAARTA-AVSCOM, Hampton, Virginia.

16. Abstract

The velocity field of a representative helicopter fuselage in a free stream is computed. Perturbation velocities due to the fuselage are computed in a plane above the location of the helicopter rotor (rotor removed). The velocity perturbations computed by a source-panel model of the fuselage are compared with experimental measurements taken with a laser velocimeter. Three paneled fuselage models are studied: fuselage shape, fuselage shape with hub shape, and a body of revolution. The velocity perturbations computed for both fuselage shape models agree well with the measured velocity field except in the close vicinity of the rotor hub. In the hub region, without knowing the extent of separation, modeling of the effective source shape is difficult. The effects of the fuselage perturbations are not well-predicted with a simplified ellipsoid fuselage. The velocity perturbations due to the fuselage at the plane of the measurements have magnitudes of less than 8 percent of free-stream velocity. The velocity perturbations computed by the panel method are tabulated for the same locations at which previously reported rotor-inflow velocity measurements were made.

17. Key Words (Suggested by Authors(s))	18. Distribution Statement
Helicopter fuselage Rotor inflow Source panel Laser velocimeter	Unclassified Unlimited Subject Category 02

19. Security Classif. (of this report)	20. Security Classif. (of this page)	21. No. of Pages	22. Price
Unclassified	Unclassified	63	A04